ON THE INTERPRETATION OF β LYRAE AND OTHER CLOSE BINARIES*

GERARD P. KUIPER

ABSTRACT

In this paper a model for β Lyrae is developed which attempts to account for the complex photometric and spectroscopic phenomena and which is consistent with dynamics.

In the introduction the dimensions of the system are discussed, and the conclusion is reached that the components have a common envelope (they form a "contact binary"). In section 2 it is shown that contact binaries with unequal components are unstable. It is shown that matter streams from A to B as long as the masses are unequal; that Δm and Δ(Spectral type) are abnormally large for the mass ratio; and that a system of currents will be set up (Fig. 4, *b*). These currents account for the satellite components of spectral lines observed near the primary minimum of β Lyrae.

If the common envelope attains great height and/or if the currents attain large velocities, ejection of matter from the outer point of B will take place. This ejection is considered to supply the source of the mysterious B_5 spectrum and to cause the asymmetry and irregularity of the photometric minimum. Ejection of another type (type A), arising in a separated binary composed of one giant and one dwarf star, is also considered, and its application to peculiar emission stars with composite spectra is stressed. The theory of both types of ejection based on Jacobi's integral is given in section 4. The orbits of ejected particles are determined in sections 5–7. Section 5 contains the first-order theory for the vicinity of the point of ejection; Figures 6 and 7 illustrate the results. Numerical integrations are used in sections 6 and 7 with Figures 8–12 showing the orbits obtained. Section 8 gives applications to β Lyrae and other stars. A schematic picture of the gaseous tail in which β Lyrae winds itself is given in Figure 13. The effect is that of a giant pinwheel with one streamer. The shadow cast by B on the streamer appears to play an important role in the spectral features, as it appears to de-ionize the gas. The change of period in β Lyrae is also considered. It appears that both the process of mass transfer from A to B and the ejection from B would tend to shorten the period. The effect on the period of the pressure at the interface of the components is examined in the addendum.

1. INTRODUCTION

It is a well-known fact that β Lyrae shows peculiar asymmetries which have not yet found an adequate explanation. These asymmetries appear in the light-curve as well as in the spectral features. We mention below the chief data and the interpretation they have thus far received.[1]

a) *The light-curve.*—Stebbins,[2] using a rubidium cell, found "a marked asymmetry of the light curve at primary minimum, the decrease of light being more rapid than the increase. This difference extends as far as the maxima on each side of the minimum, the phases of the maxima being -2.95 days and $+3.45$ days respectively." The depths of the minima were found to be 0.98 and 0.47 mag., respectively, and the maximum following the primary minimum was found to be 0.02 mag. lower than the other maximum. Such an inequality had already been suspected by K. Schwarzschild.[3]

Huffer,[4] using a potassium cell, confirmed the asymmetry of the primary minimum but found the maxima nearly equal in brightness. He obtained somewhat smaller values for the amplitudes, 0.88 and 0.40 mag. However, Smart,[5] also using a potassium cell, found amplitudes in good accord with those of Stebbins (0.97 and 0.44 mag.), so that intrinsic variations, rather than differences in the color sensitivity of the cells, may be re-

* *Contributions from the McDonald Observatory, University of Texas*, No. 28.

[1] A complete bibliography is given in the *Geschichte und Literatur des Lichtwechsels*, **2**, 156, 1920, and *Zweite Ausgabe*, **2**, 244, 1936.

[2] *Lick Obs. Bull.*, **8**, 186, 1916.

[3] *Pub. d. Kuffnerschen Sternwarte*, **5**, C 127, 1899.

[4] *Pub. Washburn Obs.*, **15**, 209, 1931.

[5] *M.N.*, **95**, 647, 1935.

sponsible for these differences in amplitude. Smart agreed with Stebbins in finding the maximum after the primary minimum about 0.02 mag. fainter than the other maximum.

A good visual light-curve has been published by Danjon,[6] who found marked changes in the light-curve during three successive observing seasons; but in all three seasons the primary minimum was strikingly asymmetrical, as is shown in Figure 1, which is reproduced from Danjon's paper. The amplitudes were 0.81 and 0.43 mag.; these values, in connection with the values found photoelectrically, suggest, as Danjon points out,[7] that the star eclipsed at primary minimum is the bluer of the two, consistent with the ratio of the surface brightnesses found from the minima.

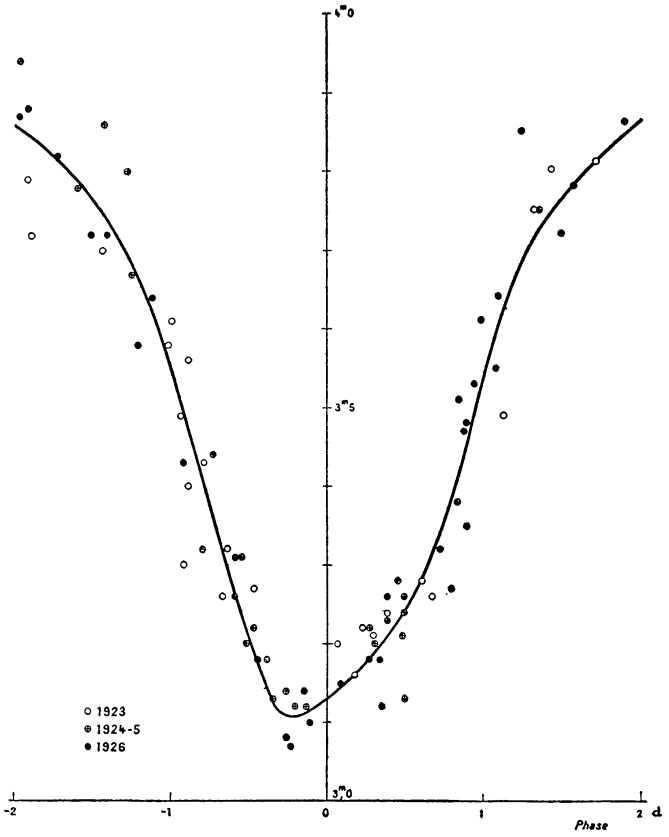

FIG. 1.—Primary minimum of β Lyrae (Danjon)

b) *The color.*—Stebbins and Huffer[8] found the color index to be $-0^m.13$ in their system, corresponding to a normal B8 star. Hall's infrared index[9] corresponds to about Ao.

Of particular interest are the color measures related to phase. The visual determinations by L. Terkan[10] were not confirmed by the more reliable photoelectric measures by Elvey[11] and by Schneller.[12] Both these observers found the binary to be reddest at primary minimum and bluest at secondary minimum. The range was found to be 0.03 mag. by Elvey (base line, 4750–4250A) and about 0.06 mag. by Schneller. These results are consistent with those by Danjon and with the ratio of the surface brightnesses.

c) *The spectroscopic observations.*—These are very numerous and need not be mentioned here in view of Dr. Struve's article in this issue.[13]

d) *The interpretation.*—Much progress in astronomy has been the direct result of attempts to interpret the observations of β Lyrae. Plassmann seems to have been the first[14] to emphasize that the double-star hypothesis, previously used to explain light-curves of the Algol type, would also be applicable to β Lyrae if tidally elongated components were assumed. That this hypothesis was correct, rather than E. C. Pickering's earlier suggestion of a single, rotating ellipsoid covered with spots,[15] was already indi-

[6] *Ann. Obs. Strasbourg*, **2**, 114, 1933.

[7] *Ibid.*, p. 130.

[8] *Pub. Washburn Obs.*, **15**, 233, 1931.

[9] *Ap. J.*, **79**, 169, 1934.

[10] *A.N.*, **226**, 345, 1926.

[11] *Ap. J.*, **81**, 173, 1935.

[12] *Kl. Veröff. Berlin-Babelsberg*, No. 17, 1936.

[13] P. 104.

[14] Cf. J. Stein, *Die veränderlichen Sterne*, **2**, 307, 1924.

[15] *Proc. Amer. Acad. Arts and Sci.*, **16**, 270, 1881.

cated by Pickering's observations of the spectrum[16] and was conclusively shown by G. W. Myers[17] with the aid of Belopolsky's radial velocities of 1892.

The first determination of the photometric elements was made by Myers,[17] who developed the necessary formulae for ellipsoidal bodies; a summary of this work was presented at the dedication of the Yerkes Observatory.[18] J. Stein found[19] that some of Myers' formulae needed correction, and he derived a new set of elements. By that time the photometric theory was practically complete.

Several photometric solutions have been published; those prior to 1924 are listed by Stein.[14] With the exception of some of von Hepperger's solutions the darker star (in front at primary minimum) was found to be the larger. This is also true of Danjon's solution[6] and of several solutions made by Sandig.[20]

TABLE 1

COMPUTED ABSOLUTE MAGNITUDES FOR β LYRAE

M_A/M_B	M_A	M_B	$M_{bol}(A)$	$M_{bol}(B)$	ΔM_{bol}	$M_{vis}(A)$
1.0	33	33	− 6.6:	− 6.6:	0.0:	− 5.6:
1.5	78	52	8.6::	7.7:	0.9:	7.6::
2.0	150	75	10:	8.6::	1.4::	9:
2.5	255	102	11:	9:	2:	10:
3.0	399	133	−11::	−10:	1–2::	−10::

The fact that the same light-curve can be explained by such widely different ratios of the radii as assumed by von Hepperger (5 and 0.6) shows that other considerations should be used as well as the conventional ones. Struve has shown[21] that the B5 spectrum is not due to a star and that only one component of the binary is visible. This means that $L_B \ll L_A$. Hence the round maxima of the light-curve are due chiefly to the elongation of A, since B is too faint. Since the composition of B and A are presumably similar, the mass-luminosity relation may be used to derive the result $M_B \ll M_A$. The considerable elongation of A then shows that the center of B must be close to A, at the most about one radius of A from A's surface. This shows that B cannot be larger than A.

A lower limit to the mass ratio and the relative size of B can be set in the following manner. From measures of the B8 component Rossiter[22] found the mass function to be $8.32\odot$. In Table 1 we give the resulting masses of the two components for different mass ratios ($B \leqslant A$), adopting $i = 90°$ in each case. (The masses so obtained will be minimum masses.) With the aid of an empirical mean mass-luminosity relation[23] bolometric magnitudes may now be derived; but, owing to the great scatter in the upper part of the mass-luminosity diagram, the star may easily differ by 1 or 2 mag. from these computed values.

We have the following information as to the true absolute magnitude of β Lyrae. Spectroscopically Struve[24] found the luminosity of the B8 component high, but less than that of Rigel, which by its double companion of type B5 may be estimated to be about −8 visually. But β Lyrae has also a visual companion. On the basis of the measures in Aitken's *Catalogue of Double Stars* (after correction for precession in angle amounting to

[16] *A.N.*, **128**, 42, 1891. Cf. also *Harvard Obs. Circ.*, No. 7, 1896; *Ap. J.*, **4**, 142, 1896.

[17] *Untersuchungen über den Lichtwechsel des Sternes β Lyrae*, Munich, 1896.

[18] *Ap. J.*, **7**, 1, 1898.

[19] *Proc. Acad. Amsterdam*, **10**, 459, 1907.

[20] *Zs. f. Ap.*, **8**, 29, 1934.

[21] *Observatory*, **57**, 265, 1934.

[22] *Pub. Michigan Obs.*, **5**, 86, 1934.

[23] *Ap. J.*, **88**, 489, 1938; 29 Canis Majoris was omitted.

[24] *Ap. J.*, **93**, 105, 1941.

$-0^{\circ}.65$ per century), the proper motions in Boss's *General Catalogue*, and the radial velocities (-19.0 km/sec for β_1 and -13 ± 5 for β_2), it is probable that the stars form a physical system. The magnitude of β_1 at maximum is 0.17 mag. fainter than the A0 star γ Lyrae according to Smart,[5] and 0.15 mag. according to Stebbins.[2] For γ Lyrae we find 3.37 IPv; hence, β(max.) = 3.53 IPv. Adopting in the bright binary $\Delta m = 3$, for reasons given later, we find for the apparent magnitude of A, 3.6.

The magnitude of the companion, β_2, is given as 7.78 in the *Henry Draper Catalogue*, as 7.40 by Danjon on the basis of measures on 17 nights,[25] and as 7.73 IPv by Mrs. Gaposchkin.[26] Danjon finds $\beta_2 - \beta_1$ (max.) = 3.95 mag.; this leads to $\beta_2 = 3.53 + 3.95 = 7.48$. We adopt 7.5. The spectral type was found to be B3 $\pm$ in the *Henry Draper Catalogue*, B8n at Victoria, and B8 by the writer. The companion is probably itself a spectroscopic binary; assuming $\Delta m = 1.0$ we find then 7.9, B8 for its brighter component. If the star is an ordinary main-sequence star, the distance modulus of β Lyrae comes out to be about 8.1; and the absolute magnitude of the B8 component of β_1, -4.5. The uncertainty of the distance modulus is probably about 1 mag. We see that this result is consistent with Struve's spectroscopic determination. A third argument leads to the same value as an upper limit; the galactic longitude being 30°, the star would be expected to show the effects of galactic rotation if the distance were as large as 1000 parsecs; actually it shows only the reflex of the solar motion, so that the distance is probably not over 400 parsecs. We have, accordingly, $M(A) = -4.5 \pm 1$.

This value, in connection with Table 1, shows that almost certainly $M_A/M_B < 2$. However, on account of the faintness of B, this ratio should well exceed unity. It seems difficult to obtain a more precise determination, and the compromise ratio, 1.5, will be adopted in the following pages. The results obtained are, with some numerical modifications, also valid for other mass ratios.

As a test of these considerations Dr. Wesselink made in 1938 a solution based upon all the major photometric series, assuming the size of B to be about two-thirds that of A. He found that a good representation could be made.[27] Later S. Gaposchkin published[28] another solution, also assuming $R_B < R_A$. But he has not used the spectroscopic observations of this star; his mass ratio $A/B = 3.8$ would lead, in connection with Rossiter's mass function, to masses thirty-seven and forty-seven times larger than those given in Gaposchkin's two solutions.

Wesselink's solution has not yet been published.[27] It is clear that the values are approximate in view of the large indeterminacy of the solution and because of the roughness of the assumption that the stars are ellipsoids with uniform disks.

On the basis of Wesselink's or Gaposchkin's solutions it follows that the components of β Lyrae are very close. The writer has pointed out[29] that for equal components built on the Roche model actual contact exists whenever $a_1/a > 0.43$ and $b_1/a > 0.38$. Here a_1 and b_1 are the true dimensions of the "ellipsoids," not necessarily those derived from the light-curve. More extensive data, also for different mass ratios, are given in Table 3. The relation between the empirical values of a_1 and b_1 and the true values cannot be found without extensive computations. It will be necessary to assume the bolometric intensity distribution over the surface to be given by the theorem $H \propto g$, although this cannot be (strictly) valid if the components are unequal; this is shown in section 2. The distribution of gravity may be obtained from Figure 3 and Tables 4*b* and 4*c*, gravity being proportional to the reciprocal of the distance between consecutive equipotential surfaces. It appears that maximum brightness will be found in a belt at right angles to the line joining the centers. The effect will be an increase of the maxima of the light-curve and con-

[25] *Op. cit.*, p. 121.

[26] *Harvard Obs. Mimeogr.*, **3**, No. 2, 1938.

[27] *Pub. A.A.S.*, **9**, 304, 1939.

[28] *Proc. Amer. Phil. Soc.*, **82**, 305, 1940; Struve, *Ap. J.*, **93**, 112, 1941.

[29] *Ap. J.*, **88**, 497 and 501, 1938.

sequently an exaggerated empirically determined ellipticity of the components. Near the minima a brightening toward the limb will be present, which, in view of the experience that darkened solutions often give larger radii than uniform solutions, may be expected to result in an underestimation of the radii. This enhances the probability that the components of β Lyrae are in contact.[30]

During the primary minimum the companion is much darker than at other phases, partly because of the low gravity at the outer point of B and partly because of obscuration to be discussed later. Hence, an exaggerated value of Δm is found from the photometric solution, and too late a spectral type is computed from the surface brightness or color.

Although we have now obtained the approximate dimensions of the system, we have, as yet, no clue to the cause of the asymmetries mentioned earlier or to the source of the B5 spectrum. It is clear that any stable system will be symmetrical with respect to the plane through the components and the rotational axis. Hence, β Lyrae cannot be a stable system. The fact that in all probability the components have a common envelope may introduce an instability. The writer had examined this question in 1932 and had found that von Zeipel's theorem cannot be valid for a binary of unequal masses with a common envelope and that a stream of matter from A to B is likely to set in until equality of mass is attained. But even this stream from A to B does not seem to be sufficient for explaining the B5 spectrum. Accordingly, a second instability should be present, which will, indeed, arise if the envelope of A and B has such heights that it fills the largest equipotential surface inclosing the two components (cf. Figs. 2 and 3). Then, at point L (corresponding to the Lagrangian point L_2 of the *problème restreint*) instability will set in, and the matter will stream out, describing a free orbit, which may be found by integration of the equations of motion of the *problème restreint*. We shall see that this mechanism provides the elements of explaining the asymmetries of the light-curve, as well as the spectral features of β Lyrae.

Before giving the analytical discussions we note another type of instability which may arise in close binaries, consisting of one large, tenuous star and another, much denser and smaller one. Instability at point G (Fig. 3) will cause matter from the large star to envelope the small one in a manner discussed later. This type of instability seems of interest in interpreting such stars as CI Cygni, AX Persei, ϵ Aurigae, VV Cephei, and perhaps also ζ Aurigae.

2. INSTABILITY IN CONTACT BINARIES

Since most of the further discussions are concerned with binaries of which the components have a common envelope, we shall introduce the short term "contact binary" for such a system; it does not mean that mere contact exists, but a common envelope as well. For equipotential (or level) surfaces inside the common envelope we shall use the term "contact surfaces."

Von Zeipel has shown[31] that, if in a rotating mass of gas (which may be a contact binary) the angular velocity ω is constant and if, further, mechanical equilibrium obtains, the total pressure P, the density ρ, and the temperature T are constant on a level surface, ϕ = constant (ϕ includes the potential due to gravity as well as that due to the centrifugal force). The argument is simply that in equilibrium

$$dP = -\rho d\phi \,. \tag{1}$$

[30] The effect of the theorem $H \propto g$ on the derived ellipticities of separated components has been studied by Luyten (*M.N.*, **98**, 459, 1938) and Russell (*Ap. J.*, **90**, 653, 1939). When this paper was practically finished, Dr. Sitterly, at the Wellesley meeting of the American Astronomical Society (September, 1940), presented computations for components of equal mass in contact. The large effect on the empirically determined radii found by Dr. Sitterly makes it practically certain that the components of β Lyrae have a common envelope.

[31] *M.N.*, **84**, 665, 1924; Eddington, *The Internal Constitution of the Stars*, pp. 282–288.

On a level surface $d\phi = 0$; and hence $dP = 0$, or $P = P(\phi)$. Solving equation (1) for ρ, we find that ρ must be a function of ϕ only and must, therefore, be constant on a level surface. Finally, the same thing holds for T, found from

$$P = \frac{R\rho T}{\mu} + \tfrac{1}{3}aT^4 , \tag{2}$$

provided the composition (entering through μ) is constant over a level surface.

It can also be shown[31] that, under the same assumption, ω = constant, the surface brightness is given by $H \propto g$.

Consider now two components having a given mass ratio and the same composition. If the components are well separated, certain empirical relations between R, L, T_e, and M exist which will be of importance later. The significance of these relations is that they give central temperatures ($\propto M/R$) which lead to an energy generation equal to L, so that equilibrium will be maintained. We shall refer to these empirical quantities as the "physical" dimensions. We have, empirically,[32]

$$\frac{L}{\odot} = \left(\frac{M}{\odot}\right)^{4\frac{1}{2}}, \qquad \frac{R}{\odot} = \left(\frac{M}{\odot}\right)^{3/4}, \qquad \text{and hence} \qquad \left(\frac{T_e}{\odot}\right)^4 = \left(\frac{M}{\odot}\right)^3, \tag{3}$$

valid for $\frac{1}{2} < M/\odot < 2\frac{1}{2}$; the third relation was verified by directly plotting T_e against M. For larger masses the exponents in the right-hand members decrease slowly as the mass increases, but their precise values become increasingly uncertain. For the interval $10 < M < 100$ we find the following approximate relations:

$$L \propto M^{2.3}; \qquad R \propto M^{0.6}, \qquad \text{and} \qquad T_e^4 \propto M^{1.1}. \tag{4}$$

On the basis of equations (3) and (4) we may compute the ratio and the sum of the radii of two components with constant average mass M_0 (to which corresponds the radius R_0). Table 2 shows the result. We note that the sum of the radii increases as the components approach equality. It is easily shown that this is generally the case whenever $R \propto M^n$, provided $0 < n < 1$.

TABLE 2

EMPIRICAL VALUES OF THE RATIO AND THE SUM OF THE RADII FOR SEPARATED COMPONENTS OF DIFFERENT MASS RATIO

M_A/M_B	R_A/R_B $\frac{1}{2}<M<2\frac{1}{2}$	$(R_A+R_B)/2R_0$ $\frac{1}{2}<M<2\frac{1}{2}$	R_A/R_B $10<M<100$	$(R_A+R_B)/2R_0$ $10<M<100$
1.0	1.00	1.000	1.00	1.000
1.5	1.36	0.996	1.28	0.995
2.0	1.68	0.989	1.52	0.986
2.5	1.99	0.982	1.73	0.977
3.0	2.28	0.975	1.93	0.968

If the two components are so close as to have a common envelope, the ratio of the radii is no longer free to adjust itself to the *physical* causes underlying equations (3) or (4) but is determined *mechanically* by the mass ratio. Strictly speaking, the ratio of the radii will depend not only on the mass ratio but also on the polytropic index of the com-

[32] *Ap. J.*, **88**, 472, 1938; 29 Canis Majoris was omitted.

ponents. Recent work[33] has empirically confirmed the older theoretical conclusion that the polytropic index of ordinary stars is close to 3. This being the case, the shape of the stars will deviate only slightly from the shape computed on the simple Roche model, as was shown by Chandrasekhar[34] for binaries with separated components. Chandrasekhar's result is obviously a consequence of the fact that for each component about 90 per cent of the mass is less than half the radius away from the center, in which region the equipotential surfaces are nearly spheres; hence, the attraction on an exterior point is very nearly the same as that valid for the Roche model. This situation is not materially changed when the components have a common envelope; hence, the approximation of the Roche model is good also in that case.

The equipotential surfaces of the Roche model are given by

$$-\Omega = \frac{1-\mu}{r_1} + \frac{\mu}{r_2} + \frac{x^2+y^2}{2}, \tag{5}$$

in which Ω is the (negative) potential and r_1 and r_2 are the distances of a point (x, y, z) to the mass centers, $M_1 = 1-\mu$ and $M_2 = \mu$; the co-ordinate system is rotating with the binary, the z-axis is the axis of rotation, the x-axis runs through the two mass centers, and the origin is at the center of gravity. The units are: the distance between the centers $= 1$; total mass $= 1$; angular velocity $= 1$ (or period $= 2\pi$).

With the aid of equation (5) we may now compute the ratio of the radii of the level surfaces; we shall call them "mechanical" radii. There are two limiting surfaces for each mass ratio, defined respectively by the Lagrangian points L_1 and L_2. L_1 gives the dimensions for the case in which the common envelope has zero height, whereas L_2 gives the maximum extent of the common envelope; if the extent should happen to be larger than defined by this limiting surface, the excess matter would stream off at L_2.

The co-ordinates of L_1 and L_2 are $y = z = 0$ and x determined by $\partial\Omega/\partial x = 0$. With the co-ordinates found, equation (5) gives the corresponding Ω_L, and then equation (5) is solved for the co-ordinates satisfying Ω_L just found. In this manner the principal axes a', a'', b, and c are found for each component and surface (a' refers to the outer dimension measured on the x-axis, and a'' to the inner dimension). Further, $b(L_1)$ and $c(L_1)$ are the y and z dimensions of the outer surface at L_1; they determine the maximum width of the bridge between the stars. As a unit we use the distance between the mass centers. On account of the pointed shape near L_1, we shall compute R from $R = \sqrt[3]{a'bc}$.

The results are found in Tables 3*a*–3*c* and are shown in Figure 2. The dots in Figure 2 mark the positions of the centers of gravity; the distance between the stellar centers was taken the same for each figure.

Before we can compare the "mechanical" dimensions of Table 3 with the "physical" dimensions of Table 2, we must know the change with changing mass ratio of the unit used in Table 3. We consider, therefore, a contact binary with total mass M = constant; with total orbital momentum $\mathcal{M}$ = constant, but with variable mass ratio. In considering $\mathcal{M}$ = constant we neglect possible variations in the rotational momentum of the two components. On the Roche model this rotational momentum would be zero, of course; actually, it is not zero but is probably small compared to the orbital momentum except when the companion has a very small mass compared to the primary. Its effect is studied below.

The total orbital momentum of the components with masses $(1-\mu)M$ and μM is, with respect to the center of gravity,

$$\mathcal{M} = (1-\mu)M\mu^2a^2\omega + \mu M(1-\mu)^2a^2\omega = \mu(1-\mu)Ma^2\omega = \text{constant}.$$

[33] Cowling, *M.N.*, **98**, 734, 1938; Russell, *op. cit.*, p. 641.

[34] *M.N.*, **93**, 539, 1933 (cf. Fig. 9, p. 566, and pp. 569–571).

At any time ω is found from Kepler's third law, $\omega^2 a^3 = GM$. After elimination of ω we find

$$\mu^2(1 - \mu)^2 a = \text{constant}, \tag{6}$$

and for the period P

$$\mu^3(1 - \mu)^3 P = \text{constant}. \tag{7}$$

From equation (6) it follows that a has a minimum for $\mu = \frac{1}{2}$ and starts from infinity with $\mu = 0$. For very small μ-values, however, the rotational momentum of the primary will

TABLE 3*a*

PROPERTIES OF THE INNERMOST CONTACT SURFACE

M_A/M_B	μ	L_1	$\Omega(L_1)$	a_1'	a_1''	b_1	c_1	a_2'	a_2''	b_2	c_2
1.0....	1/2	0.00000	2.0000	0.405	0.500	0.374	0.356	0.405	0.500	0.374	0.356
1.5....	2/5	.14162	1.9905	.442	.542	.412	.390	.370	.458	.337	.323
2.0....	1/3	.23742	1.9728	.468	.571	.440	.414	.346	.429	.313	.300
2.5....	2/7	.30723	1.9537	.488	.593	.462	.433	.327	.407	.295	.283
3.0....	1/4	0.36074	1.9353	0.505	0.611	0.480	0.448	0.313	0.389	0.280	0.269

TABLE 3*b*

PROPERTIES OF THE OUTERMOST CONTACT SURFACE

M_A/M_B	L_2	$\Omega(L_2)$	a_1'	b_1	c_1	$b(L_1)$	$c(L_1)$	a_2'	b_2	c_2
1.0.....	1.1984	1.7284	0.698	0.482	0.437	0.326	0.289	0.698	0.482	0.437
1.5.....	1.2308	1.7595	.589	.502	.456	.295	.265	.631	.427	.392
2.0.....	1.2490	1.7737	.583	.518	.471	.273	.246	.582	.390	.361
2.5.....	1.2597	1.7795	.586	.531	.481	.255	.231	.545	.363	.337
3.0.....	1.2659	1.7806	0.590	0.542	0.492	0.243	0.219	0.516	0.342	0.318

TABLE 3*c*

"RADII" OF THE INNER CONTACT SURFACES

M_A/M_B	R_A	R_B	R_A/R_B	R_A+R_B
1.0.....	0.378	0.378	1.00	0.756
1.5.....	.414	.343	1.21	.757
2.0.....	.440	.319	1.38	.759
2.5.....	.460	.301	1.53	.761
3.0.....	0.477	0.287	1.66	0.764

become of importance. The decrease of a with increasing μ is quite appreciable even for moderate values of μ; for instance, if we start with $M_A/M_B = 3$ and if later the masses have become equal, the distance of the centers will have decreased by the factor 9/16. By (7) the period of revolution will have decreased by 27/64. Assuming that at all times the periods of rotation are very nearly equal to the period of revolution, we find that, as the components approach equality, the rotational momentum increases; this is shown below. Hence, the orbital momentum decreases as $\mu \rightarrow \frac{1}{2}$, which proves that, in reality, the

distance between the components decreases even more rapidly than according to equation (6) and the period of revolution will decrease more rapidly than according to equation (7).

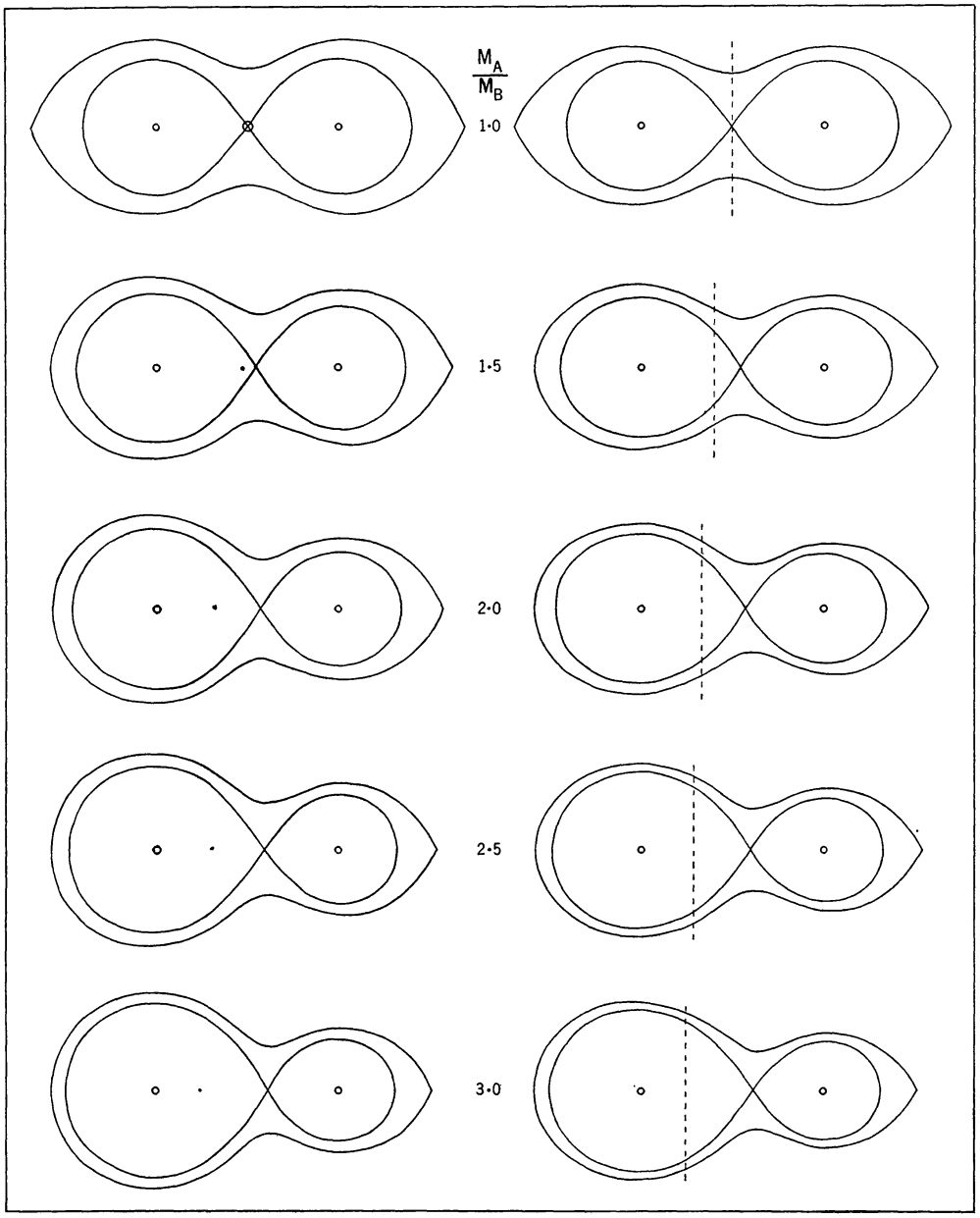

FIG. 2.—Inner and outer contact surfaces for different mass ratios. Sections in xy plane left, in xz plane right. Axes of rotation (through centers of gravity) shown as broken lines.

If γR is the radius of gyration of a star, its rotational momentum is $\gamma^2 R^2 M\omega$; the total rotational momentum of the components is $\gamma^2\omega[R_1^2 M_1 + R_2^2 M_2]$. Putting, as before, $R = M^n$ $(\frac{1}{2} < n < \frac{3}{4})$ and using equation (7), we find that the total rotational momentum is proportional to

$$\gamma^2\mu^3(1-\mu)^3\{(1-\mu)^{1+2n} + \mu^{1+2n}\} .$$

Evaluating this function for $\mu = \frac{1}{4}$ and for $\mu = \frac{1}{2}$, we find that in the latter case the rotational momentum is 1.90 or 1.62 times larger than in the former, depending upon whether we use the one or the other extreme value of n, $\frac{1}{2}$ or $\frac{3}{4}$. This proves the statement made above, at least if the approximation of ω = constant throughout the components is adequate. In view of the strong tidal forces, this approximation should be valid for the bulk of each star; the very central region, as well as the outermost parts (discussed below), may deviate, but their contribution to the momentum is slight.

In view of the considerable decrease in distance between the mass centers as the components approach equality and the comparatively small change in the sum of the "physical" radii shown in Table 2, it seems probable even at this stage that, if two unequal components once have a common envelope, they will continue to do so and that the envelope will become increasingly prominent. But, since the stars will be unable to retain their physical radii, we have to study the "adjustments" to the radii before certainty can be obtained as to the future of the envelope.

Consider, first, two separated components of masses M_1 and M_2, having "physical" radii R_1 and R_2, and internal energies $E_1(M_1, R_1)$ and $E_2(M_2, R_2)$. Compare this combination with a contact binary with the same masses but "adjusted" radii, $R_1 + h_1$ and $R_2 + h_2$. It seems probable that the adjustments in the radii will be made in such a way that the total energy of the system does not change. If this assumption is correct, we have

$$E_1(M_1, R_1 + h_1) + E_2(M_2, R_2 + h_2) = E_1(M_1, R_1) + E_2(M_2, R_2) \, . \tag{8}$$

After a Taylor expansion this reduces to (retaining only first-order terms)

$$h_1 E'(M_1, R_1) + h_2 E'(M_2, R_2) = 0 \, , \tag{9}$$

in which the derivatives are taken with respect to the radius. The internal energy is proportional to M^2/R; the constant of proportionality will be the same for the two components if they have the same polytropic index and also the same ratio β between the gas pressure and the total pressure.[35] Equation (9) then becomes

$$h_1 \frac{M_1^2}{R_1^2} + h_2 \frac{M_2^2}{R_2^2} = 0 \, . \tag{10}$$

It is of interest to note that one finds the same equation by considering the work done in displacing against gravity a small fraction, α, of each mass in opposite directions, the mean displacements being h_1 and h_2: $h_1 \alpha M_1 g_1 + h_2 \alpha M_2 g_2 = 0$, and $g \propto M/R^2$.

Equation (10) gives only the *ratio* of the increments of the radii. In order to obtain an indication of their absolute amount, we shall assume that the "mechanical" radii can be reached, starting from the "physical" radii, by the same adiabatic change (eq. [8]). Obviously, the radii adopted by the contact binary will be intermediate between the physical and the mechanical radii; we shall call them "compromise" radii.

Because of the ill-defined shape of the "compromise" binary, we shall examine the question of whether the common envelope will continue to exist by comparing the "physical" with the "mechanical" dimensions. Equation (10) plus the known ratio of the radii fixes the mechanical dimensions for each mass ratio,

$$\frac{(R_p + h)_1}{(R_p + h)_2} = \frac{(R_m)_1}{(R_m)_2} = \left(\frac{M_1}{M_2}\right)^m , \tag{11}$$

[35] Chandrasekhar, *Stellar Structure*, pp. 230–232, 1939.

in which R_p and R_m are the physical and mechanical radii, and the exponent m is found, from Table 3*c*, to be about 0.46. Using now in equations (10) and (11) the empirical relation $R_p = cM^n$ ($n = \frac{3}{4}$ for dwarfs, and about 0.6 for massive stars), we are able to solve for h_1 and h_2 in terms of M_1 and M_2. Then, putting $M_1 = M_0(1 + \delta)$ and $M_2 = M_0(1-\delta)$ we find, up to the second power of δ,

$$h_2 = R_0(n - m)\delta\{1 + 2(1 - n)\delta\} ; \qquad h_1 = -R_0(n - m)\delta\{1 - 2(1 - n)\delta\} , \quad (12)$$

in which R_0 is the physical radius corresponding to M_0 ($R_0 = cM_0^n$).

We consider first the change in the sum of the radii over the sum of the physical radii

$$\frac{h_1 + h_2}{2R_0} = 2(1 - n)(n - m)\delta^2 . \quad (13)$$

If $\delta = \frac{1}{2}$, or $M_A/M_B = 3$, and $n = \frac{3}{4}$, the right-hand member of equation (13) is 0.036; if $n = 0.6$, the right-hand member is 0.028. If we add these figures to the sum of the physical radii found from Table 2 (0.975 and 0.968, respectively), we find 1.011 and 0.996 for dwarfs and massive stars, respectively. This shows that the sum of the "adjusted" mechanical radii (adjusted by means of eq. [10]) remains very nearly constant in comparison with R_0, i.e., in absolute measure, if the masses approach equality. Now we see from Table 3*c* that the sum of the mechanical radii remains very nearly constant if it is expressed in terms of the distance between the mass centers. Hence, if the degree of contact were to remain the same during the process of mass transfer, the distance of the mass centers would have to remain very nearly the same (more precisely: for dwarfs the change would have to be by the factor 0.999, and for massive stars by the factor 1.014, for a change of mass ratio from $A/B = 3$ to 1). Actually, as we have seen, the distance of the mass centers changes by a factor less than $9/16 = 0.562$. Hence, *the degree of contact increases very considerably during the process of mass transfer*—so much, in fact, that if the process should start with masses sufficiently different, instability on the outermost point of the companion would necessarily set in before equalization of masses would be attained (cf. Table 3, and Figure 2).

Since $n > m$, we see by equation (12) that the primary will be compressed and the companion expanded over the physical dimensions. The ratio h_2/h_1 is found to be

$$-\frac{h_2}{h_1} = 1 + 4(1 - n)\delta , \quad (14)$$

which may also be directly obtained from equation (10). It shows that the secondary always makes a larger adjustment to its radius than the primary. If $n = \frac{1}{2}$, we find from equation (10) that the changes in dimension are such that the total *volume* of the components remains the same; if $n = \frac{2}{3}$, the total *surface area* remains unchanged. If $n = 1$, the sum of the *radii* would remain unchanged; but n is never so large.

As was suggested before, the true dimensions of the components will be intermediate between the physical and mechanical dimensions. This appears inevitable because, first, the physical dimensions are ruled out, since they would not provide mechanical equilibrium, the outer surface not being an equipotential surface; this is a consequence of n being larger than m. But neither could an equipotential surface be the true boundary, because it would require such a contraction of A, and expansion of B, that the internal temperatures ($\propto 1/R$) would change materially, and even more so the energy generations ($\propto T^{18\pm}$). These changes would tend to restore, at least in part, the physical dimensions. Even after a long time the mechanical dimensions could not become equilibrium dimensions, because the empirical relations between L, R, and M would not exist. These em-

pirical relations are equivalent to such theoretical relations as are given by Gamow,[36] based on the carbon-nitrogen cycle of nuclear transmutations in stellar interiors. This shows that the true dimensions of the components must be intermediate between the two extremes considered.

This result leads at once to several important conclusions. The most important one is that on the outer equipotential surfaces the pressure could not be constant; in fact, some of these surfaces will be inside the envelope of A but already outside B. This result is contradictory to that derived on page 137 on the basis of constant angular velocity. Hence, ω cannot be constant throughout, particularly in the envelope where these contradictions occur. The pressure gradient along the level surfaces will cause matter to stream from A to B. Obviously, this current will be the more intense, the greater the disparity between the physical and the mechanical dimensions, or, in other words, the larger the mass ratio A/B. It will further depend on the extent of A beyond the lowest "contact surface."

Since the components assume compromise dimensions, R_A is smaller than normal; hence, the central temperature of A will be increased, and the energy generation will be considerably increased. Hence, L_A is increased, and also $T_e^4 \propto L/R^2$ (for two reasons). Opposite results follow for B. Hence, the magnitude difference, Δm, is increased considerably above the value normal for the mass ratio; also the ratio of the surface brightnesses and the difference in spectral type. All these results are of interest in connection with β Lyrae, where Δm is definitely too large for the mass ratio.

We shall now show that the greatest ratio between the pressures in A and B exists along the level surfaces in the outer parts of the common envelope; but the greatest pressure gradient, being determined by the difference in pressure, will be further down inside the envelope. Both statements follow from the fact that the pressure gradient is smaller in the envelope of A than in that of B. This results from the following:

We have shown that the effective temperatures of the components will differ more than according to the equilibrium relations (3) or (4). Hence, for components of unequal mass, $T_e(1) \gg T_e(2)$. Consider first isothermal atmospheres; we shall consider the pressure gradients along the "b"-axes, where the deviations from equilibrium will not be very large. Neglecting radiation pressure, we have

$$p = p_0 e^{-(\mu g h/RT)}, \tag{15}$$

in which μ is the mean molecular weight, g the surface gravity, and the co-ordinate h is measured in an outward direction from the level with pressure p_0. For the "compromise" radii $g_1 \cong g_2$; and a high value of T will result in a low value of μ, although, owing to the great abundance of hydrogen in stellar atmospheres, the variation in μ will not be great. The exponent in equation (15) is clearly less for the primary, having the higher temperature.

Now, extending the computations to greater depths, we have the standard equations

$$\frac{dP}{dh} = -g\rho, \tag{16}$$

$$P = \frac{R}{\mu}\rho T + \tfrac{1}{3}aT^4, \tag{17}$$

$$T^4 = T_0^4(1 + \tfrac{3}{2}\tau), \tag{18}$$

$$d\tau = -\frac{\kappa_0 \rho^2 dh}{T^{3.5+\Delta}}. \tag{19}$$

In equation (18) we have assumed that the layers considered are not so thick that the approximation of plane-parallel layers is invalid; then, also, g = constant. Furthermore,

[36] *Ap. J.*, **89**, 130, 1939.

equation (19) assumes that the hydrogen content of the two envelopes is the same;[37] the exponent Δ will take care of the principal deviations from Kramers' law in the envelope. The solution of these four equations is particularly simple if we assume a constant ratio β between the gas and the total pressure; equation (17) then becomes $\beta P = R\rho T/\mu$.

First we keep equation (18) and eliminate ρ; then we eliminate τ and get

$$\frac{dP}{P} = -B\frac{dh}{T} \qquad (20) \qquad \text{and} \qquad AT^{8.5+\Delta} \cdot dT = -P^2 \cdot dh\,, \qquad (21)$$

in which

$$B = \frac{g\beta\mu}{R} \qquad \text{and} \qquad A = \frac{8}{3} \cdot \frac{R^2}{T_0^4 \kappa_0 \beta^2 \mu^2}\,. \qquad (22)$$

Now, eliminating dh from equations (20) and (21) and neglecting $T_0^{8.5+\Delta}$ in comparison with $T^{8.5+\Delta}$, we have

$$\frac{8.5+\Delta}{2} P^2 \cong ABT^{8.5+\Delta}\,, \qquad (23)$$

which is valid except at the very boundary. Putting, for brevity, $8.5 + \Delta = 2F$ (where $F \backsim 4$), we have by equations (20) and (23)

$$dT = -\frac{B}{F}\,dh \qquad (24') \qquad \text{or} \qquad T = T_* - \frac{B}{F}\,h\,, \qquad (24)$$

if $T_* = T(h = 0)$. By equation (23) we then have

$$P = \sqrt{\frac{AB}{F}}\left(T_* - \frac{B}{F}\,h\right)^F\,. \qquad (25)$$

Now compare the two components on the b-axes. Assuming Δ to be the same for the two stars, the pressure gradients given by equation (25) will depend on A and B. The values of g are almost identical. The value of μ need not be the same; but if hydrogen is as prominent in the outer parts as in the sun and in other stars (H: metals about 2000 by number), μ will be close to $\frac{1}{2}$ in either case because the ionization must soon be nearly complete. If, further, $\beta_1 \cong \beta_2$, $B_1 \cong B_2$. But $A \propto T_e^{-4}$.

Suppose, now, that the pressures of the two components were equal at the innermost "contact surface," where the densities are highest, and that we count h from this surface upward. Then by assumption $P_1^* = P_2^*$, and by equation (25) $A_1 T_{1*}^{2F} = A_2 T_{2*}^{2F}$; hence,

$$T_* \propto T_e^{2/F}\,. \qquad (26)$$

The value of T_* is, therefore, higher for A than for B, and by equation (24') this is true for any value of h in the envelope.[38] We obtain here another interesting contradiction to the results derived on page 137 on the assumption of ω = constant, quite independently from the previous discussion. Of course, this contradiction results from $T_e(1) \gg T_e(2)$, which, in connection with $g_1 \cong g_2$, is already in itself a contradiction of von Zeipel's theorems.

[37] Chandrasekhar, *Stellar Structure*, p. 293, 1939.

[38] Equal steps in h mean nearly equal steps in potential because $g_1 \backsimeq g_2$.

Since $T_{1*} > T_{2*}$, it follows from equation (24) that the envelope of A extends to a greater height than B above the level for which by hypothesis $P_1 = P_2$; the ratio of the heights is $[T_e(1)/T_e(2)]^{2/F}$. Now, expressing h in terms of the height of B's envelope, we have by equations (25) and (26)

$$\frac{P_1}{P_2} = \left[\frac{1 - hf}{1 - h}\right]^F, \qquad \text{if} \qquad f = \left[\frac{T_e(2)}{T_e(1)}\right]^{2/F} < 1 . \tag{27}$$

This shows that in the whole envelope above the level where the pressures are equal, ($0 < h < 1$), the pressure in A is larger than in B, so that matter must flow from A to B.

Summarizing the results of this section, we find:

1. If two components of unequal mass are so close as to have a common envelope, the angular velocity ω cannot be constant throughout the system, because, even if for some layer inside the common envelope the pressures were equal (as demanded by ω = constant), the pressure above that level would be larger in A than in B, causing a stream of matter to flow from A to B.

2. Owing to the fact that the equilibrium ("physical") radii of stars differ more than the "mechanical" radii of a contact binary, the true dimensions of the components will be intermediate between them. This causes A to be the larger, and B smaller, than the "average" level boundary surface. Hence, the pressures in the envelope will be larger in A than in B on the same level surface. This applies probably even to the deepest-level surface of the common envelope, so that the stream from A to B is probably more violent than that caused by the effect mentioned under 1.

3. Since A is smaller and B larger than their respective "physical" radii, the internal temperatures and luminosities of the components differ more than normal for their mass ratio; Δm and Δ(Sp.) are both abnormally large.

4. During the mass transfer from A to B the components draw closer together, increasing the extent of the common envelope. This may lead to an instability on the outside of B (at the Lagrangian point L_2). Obviously, the decrease in distance will not be quite as much as computed on dynamical grounds alone, because of the pressure at the interface.

The *origin* of a contact binary may be conceived in two ways:

a) The binary had so little initial angular momentum that it could not develop two separated components with radii appropriate for their masses and composition. This is no more mysterious than the formation of a binary with a larger angular momentum and consequent larger separation.

b) The process of stellar evolution (diminishing H content) may have caused an increase in the radii; this would cause the rotational momentum to increase and the orbital momentum to decrease, which would result in a decreased distance between mass centers. The two effects would be additive.

3. CURRENTS IN CONTACT BINARIES

We shall now try to find some properties of the motion of the matter streaming from A to B. Although the general problem is very complex, some results may easily be obtained.

It will be useful to have, first, more details about the shape of the equipotential surfaces because they show at once, for instance, the distribution of gravity. We have derived for one case, $M_A/M_B = 1.5$ (or $\mu = 0.4$), the cross-sections with the xy-plane of four crucial surfaces. The value of μ chosen is of no particular consequence, as all the significant features are also present for different mass ratios. The result of the computations is found in Tables 4*a* and 4*b* and is shown in Figure 3. In addition, data for the xz-plane are given in Table 4*c*.

We note that there are three points on the x-axis for which $\partial\Omega/\partial x = 0$; they are B, G, and L of Figure 3. They correspond to the Lagrangian straight-line solutions of the three-body problem; and equation (5), giving the equipotential surfaces, corresponds to the surfaces of zero velocity defined by Jacobi's integral. We shall make use of these circumstances in determining the motion of ejected matter.

TABLE 4*a*

VALUES OF x FOR CRUCIAL VALUES OF $-\Omega$

($M_A/M_B = 1.5$)

Point	$-\Omega$	x	Point	$-\Omega$	x
A	1.760	−1.370	G	1.990	+0.142
B	1.690	1.162	H	2.167	0.279
C	1.760	0.989	I	2.167	0.909
D	1.990	0.842	K	1.990	0.970
E	2.167	−0.781	L	1.760	+1.231
F	2.167	0.000			

TABLE 4*b*

VALUES OF $\pm y$ FOR GIVEN VALUES OF x AND $-\Omega$

($M_A/M_B = 1.5$)

x	$-\Omega$					
	2.167	1.990	1.760	1.690	1.690	1.760
−1.3	.....	.....	.....	.....	.....	0.519
−1.2	.....	.....	.....	.....	0.444*	0.767
−1.1	.....	.....	.....	0.138	0.763	0.932
−1.0	.....	.....	.....	.285	0.928	1.056
−0.8	.....	0.178	0.375	.450	1.143	1.236
−0.6	0.313	.371	.485	.530	1.280	1.358
−0.4	.365	.412	.502	.535	1.368	1.438
−0.2	.308	.362	.458	.496	1.418	1.485
0.0	.000	.202	.354	.404	1.436	1.501
+0.2	.....	.087	.300	.355	1.422	1.488
+0.4	.222	.280	.380	.422	1.375	1.444
+0.6	.292	.337	.427	.466	1.290	1.366
+0.8	0.224	0.287	.406	.460	1.157	1.246
+1.0	.....	.....	.305	.415	0.941	1.065
+1.1	.....	.....	.211	0.425	0.759	0.938
+1.2	.....	.....	0.055	.....	.....	0.758
+1.27	.....	.....	.....	.....	.....	0.545†

* Second value, 0.141. † Second value, 0.105.

The points B, G, and L have the x-co-ordinates given in Table 4*a;* the values of $-\Omega$ are 1.690, 1.990, and 1.760, respectively. At the center of gravity, F, $-\Omega = 2\frac{1}{6}$. The four surfaces defined by these values of the potential are those considered here.

The largest possible envelope of a contact binary will extend to the surface passing through L. If the system were larger, matter would flow off at L because, in the rotating frame of reference, gravity reverses itself there (or, in a stationary frame, the centrifugal force becomes larger than gravity).

Currents are defined as large-scale differential motions with respect to the condition ω = constant. If ω = constant, the level surfaces are also surfaces of constant P, ρ, and

T. In the preceding section we found several contradictions to these consequences of ω = constant, so that currents must exist.

On a "contact surface" the pressure is higher in A than in B. A stream of matter must therefore flow from A to B, although conceivably part of this stream may return; in that case the outgoing stream must be stronger than the returning stream. If gas and radia-

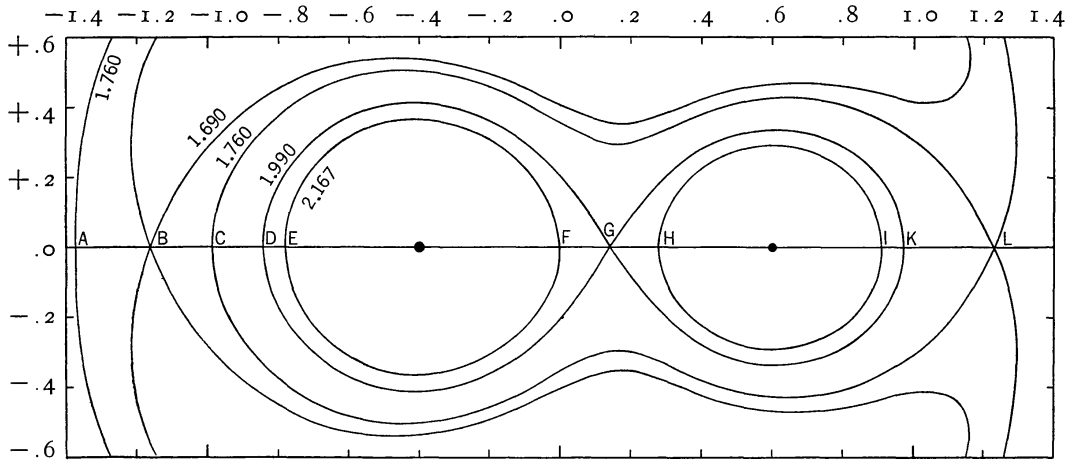

FIG. 3.—Four crucial equipotential curves in xy plane for $\mu=0.4$

TABLE 4c

VALUES OF $\pm z$ FOR GIVEN VALUES OF x AND $-\Omega$

($M_A/M_B=1.5$)

x	$-\Omega$			x	$-\Omega$		
	1.990	1.760	1.690		1.990	1.760	1.690
−1.6	.....	1.392	1.860	+0.3	0.194	0.308	0.344
1.5	.....	0.727	1.048	0.6	.323	0.391	0.418
1.45	.....	0.483	0.789	0.9	0.188	0.323	0.355
1.4	.....	0.252	0.583	1.1	.....	0.169	0.289
1.3	.....	.....	0.279	1.3	.....	0.121	0.384
1.0	.....	.....	0.213	1.4	.....	0.371	0.621
0.7	0.287	0.389	0.425	1.5	.....	0.749	1.052
−0.4	.390	0.456	0.480	+1.6	.....	1.389	1.852
0.0	0.196	0.319	0.358				

tion pressures were absent, and also viscous forces, the motion of the stream would be determined by the equations of motion of the *problème restreint*. These equations are[39]

$$\left.\begin{aligned} \ddot{x} &= 2\dot{y} + x - (1-\mu)\frac{x-x_1}{r_1^3} - \mu\frac{x-x_2}{r_2^3} \\ \ddot{y} &= -2\dot{x} + y - (1-\mu)\frac{y}{r_1^3} - \mu\frac{y}{r_2^3} \\ \ddot{z} &= -(1-\mu)\frac{z}{r_1^3} - \mu\frac{z}{r_2^3} \end{aligned}\right\} \quad \left(\text{with } \begin{aligned} r_1^2 &= (x-x_1)^2 + y^2 + z^2, \\ r_2^2 &= (x-x_2)^2 + y^2 + z^2 \end{aligned}\right). \qquad (28)$$

[39] E.g., Moulton, *Introduction to Celestial Mechanics* (2d ed.), p. 280, 1914.

If $z = 0, \ddot{z} = 0$; hence, if also $\dot{z} = 0$, the motion will remain in the xy-plane. If $z \neq 0$, we see that points symmetrical with respect to the xy-plane having symmetrical motions (i.e., the same $\dot{x}$ and $\dot{y}$; and $\dot{z}_1 = -\dot{z}_2$) will also have symmetrical accelerations. Hence, the motions will remain symmetrical with respect to the xy-plane. Adding, now, the effects of the pressure gradient and viscous forces, this symmetry will not be disturbed—not, at least, if we start with the reasonable assumption of initial symmetry in the distribution of matter. Hence, the principal current should be symmetrical with respect to the xy-plane.

Since two symmetrical currents in the z-direction would lead to a dissipation of energy not present in currents parallel to the xy-plane, it is very probable that the latter are the most important currents. We shall find their chief features by considering the motion in the xy-plane itself. Furthermore, in eclipsing binaries this is the plane in which observations may be made.

Consider the point G (Fig. 3), and assume that the pressure difference between the components gives rise to a current through G parallel to the x-axis ($\dot{x} = v$; $\dot{y} = 0$). Equation (28) now becomes

$$\ddot{x} = \text{finite}; \qquad \ddot{y} = -2v. \qquad (28')$$

The pressure gradient at G will have an x-component, but none in y, if we start from a symmetrical distribution of matter. Also, the viscous forces act only in the direction of the current, i.e., in x. Hence, these additional forces affect in equation (28′) only $\ddot{x}$. The current is going to be deflected in the $-y$-direction, owing to the well-known Coriolis force given by the second part of equation (28′).

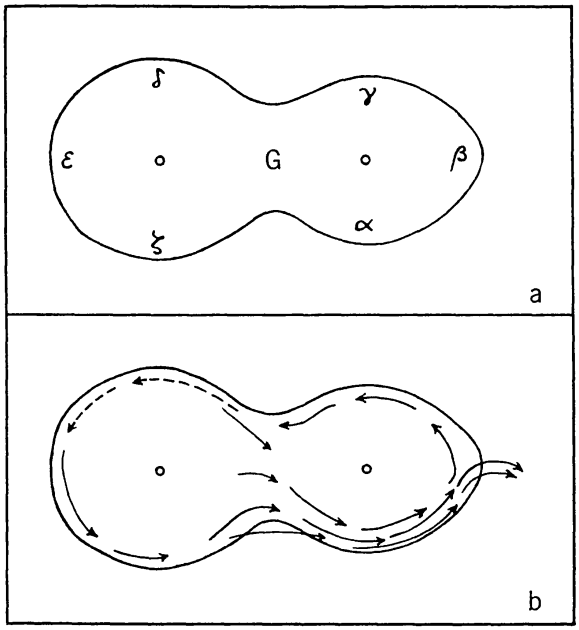

FIG. 4.—Currents in contact binaries; xy plane

The same conclusion can be reached for any point on the "interface" between the components. As this surface we may define the locus of points passing through G where the potential gradient is perpendicular to the x-axis. Consider two symmetrical points, $x_1 = x_2; y_1 = -y_2 = y$, and again $\dot{x} = v, \dot{y} = 0$. We now have $\ddot{x}_1 = \ddot{x}_2$; but $\ddot{y} = -2v \pm fy$, in which f is the same factor in the two cases. Starting again with a symmetrical distribution of matter with respect to the x-axis, there will be a component of the pressure gradient in both co-ordinates, being equal and of the same sign in the x-direction and equal but of opposite sign in the y-direction; its effect may be added to fy above. Hence, all currents passing the interface parallel to the x-axis are deflected in the $-y$-direction. The current from G (which will have a tendency to follow level surfaces) will therefore go principally in the direction of α (cf. Fig. 4, a) and not in the direction of γ.

Given a strong current near α in the $+x$-direction, what will its course be? Numerical integrations in section 7 show that, if the speed is below a certain value, the matter will go around the companion in the sense α, β, γ. If, however, the speed is large, the matter will fly off near β. The returning stream (in the $-x$-direction) will experience a Coriolis force in the $+y$-direction. Above G the returning stream meets the outgoing stream; but, owing to the opposite deflections in the y-direction, it is probable that part of the current

through γ survives and will go around the primary to join afterward the main stream near G.

The picture found is illustrated schematically in Figure 4, *b*. It is of great interest that Struve has actually identified these currents in β Lyrae.[40] The current near α has a velocity (in a stationary frame) of about 300 km/sec; this current is very prominent. Near γ a weaker returning current is observed with a speed of about 200 km/sec. Since the velocities were measured when these currents projected themselves on the primary, it is obvious that the figures quoted apply without alteration to the rotating frame in which these phenomena were considered here.

The true dimensions of the components are not represented by one level surface; hence the matter coming from the outer layers of A would practically find a vacuum over B. This is another reason why the current at α is more pronounced than that at γ.

The considerable velocities present in β Lyrae, in connection with the transverse effect of the Coriolis force, will make large departures possible from level surfaces, particularly where the potential gradient is low. This will be the case in the vicinity of point G as well as of L (cf. Fig. 3). In fact, the absorption due to the currents measured by Struve seems to be most prominent between G and α, and G and γ, respectively (Fig. 4, *a*); the discrepancy in the radii and the low effective gravity would combine to favor this region for the formation of extensive masses of gas of low density, as evidenced by the observed absorptions.

4. EJECTION OF MATTER FROM CLOSE BINARIES

In the introduction we noted two possible ways in which matter could be ejected from one of the components of a close binary; we shall refer to them as type A and type B of ejection. Type A takes place from the larger component (A), and AX Persei seems to be a good example; type B takes place on the outside of the smaller component (B) and is to be identified with β Lyrae. As is seen from Figure 3, type B arises when a contact binary "overflows" the level surface through L; type A arises if one of the components overflows the level surface through G and if the other component is much smaller than it would be according to this surface.

Some general remarks about the motion of the ejected material may readily be made on the basis of Jacobi's integral,[41]

$$\tfrac{1}{2}v^2 = \frac{1-\mu}{r_1} + \frac{\mu}{r_2} + \frac{x^2+y^2}{2} - C\,, \tag{29}$$

in which v is the velocity of the ejected particle in the rotating frame of reference. The unit of velocity is the relative orbital velocity in the binary; for β Lyrae, adopting $M_A/M_B = 1.5$, this is about $2.5 \times 183 = 460$ km/sec. For moderate velocities of ejection, v_0, the quantity $\frac{1}{2}v_0^2$ is therefore quite small. For instance, if in β Lyrae $v_0 \leqslant 50$ km/sec, $\frac{1}{2}v_0^2 \leqslant 0.006$, which is small compared to the constant C in (29); C equals 1.990 for point G of Figure 3, and 1.760 for L, if $v_0 = 0$ in both cases.

Now consider ejection either of type A or of type B. The value C_0 of C in (29) depends on v_0 but will be only slightly less than the value computed for $v_0 = 0$. Since always $v^2 > 0$, we have for the future co-ordinates of the ejected material the inequality

$$\frac{1-\mu}{r_1} + \frac{\mu}{r_2} + \frac{x^2+y^2}{2} > C_0\,, \tag{30}$$

which means that the matter has to remain on one side of the "surface of zero velocity" defined by equation (30) after making the inequality into an equality. These limiting

[40] Cf. p. 114.

[41] Easily derived from eqs. (28); cf. Moulton, *loc. cit.*

surfaces are illustrated in Figure 5; they are valid for small v_0. If v_0 should be large, the permitted regions will extend somewhat beyond the boundaries drawn, as is seen by comparison with Figure 3; the extensions are indicated by broken lines in Figure 5. The broken lines given for type B show the surface $-\Omega = 1.690$ and correspond therefore to $\frac{1}{2}v_0^2 = 1.760 - 1.690 = 0.070$, or $v_0 = 0.374$, i.e., about 170 km/sec in case of β Lyrae.

Ejection of type A appears to have the curious result that the large star ("M" star) makes a shell or ring around the small ("B") star. It is possible to derive from Jacobi's integral the approximate radius of the ring. If v_0 is not too large, the ejected particles start near their surface of zero velocity, and the orbit around B will therefore be eccentric. On account of the perturbations due to A, this orbit will have a rotation of the line of apsides; in addition the frame is rotating. Orbits of different particles will therefore intersect, and the result of collisions will be that a nearly circular ring will be formed with a radius determined by the available energy.

Let the radius of the final, common orbit be a, and assume a to be a small quantity of the first order (the unit is the distance AB). The mass of B being μ, the angular velocity in a fixed frame is found from Kepler's third law: $\omega^2 a^3 = \mu$. We shall see later that the motion around B is direct; hence the angular velocity in the rotating frame is $\omega_r = \omega - 1$. The left-hand term of equation (29) therefore equals

$$\tfrac{1}{2}v^2 = \tfrac{1}{2}a^2\omega_r^2 = \tfrac{1}{2}a^2(\mu^{1/2}a^{-3/2} - 1)^2 . \tag{31}$$

The right-hand member of equation (29) may be written as $U - C$, in which C is determined from the boundary condition of $\frac{1}{2}v_0^2 = U_0 - C$, and in our approximation

$$U = \frac{1-\mu}{1} + \frac{\mu}{a} + \frac{(1-\mu)^2}{2} . \tag{32}$$

Hence, a is found from

$$\tfrac{1}{2}a^2(\mu^{1/2}a^{-3/2} - 1)^2 = \frac{1-\mu}{1} + \frac{\mu}{a} + \frac{(1-\mu)^2}{2} - U_0 + \tfrac{1}{2}v_0^2 . \tag{33}$$

For $\mu = 0.4$ and $v_0 = 0$ we find $a = 0.21$; the value of a increases for increasing v_0 and is found to be 0.25 if $v_0 = 0.5$. These values of a are necessarily rough because of the approximations used. A precise result may be obtained by deriving the variational orbit around the companion having the Jacobian constant determined by the boundary conditions at the point of ejection. For the case of equal masses and small v_0 we find, by interpolation in a diagram by E. Strömgren,[42] that $a \cong 0.25$; while for the extreme case of $M_A/M_B = 10$, considered by G. H. Darwin,[43] we find that $a \cong 0.13$. The approximate result obtained above for $\mu = 0.4$ is hereby confirmed.

The correct order of magnitude for a is already obtained from the two-body problem, in which case the total energy in a circular orbit equals the potential energy at double the distance. According to this rule, the radius of the gaseous ring should be about half that of the curve of zero velocity, or about 0.2 for small v_0.

We may now take into account radiation pressure by a small, but hot, secondary. The example of the two-body problem would lead to the same radius of the ring as before if the radiation pressure does not exceed gravity; because, if α is the ratio between radiation pressure and gravity, the only effect will be to reduce the effective mass of the attracting star by the factor $(1-\alpha)$. In the three-body problem considered, the ring would

[42] *Bulletin astronomique*, **9**, 112, Fig. 23, 1935. The Jacobian constant is 16.

[43] *Scientific Papers*, **4**, 70, Pl. IV. The appropriate Jacobian constant is 40.1821.

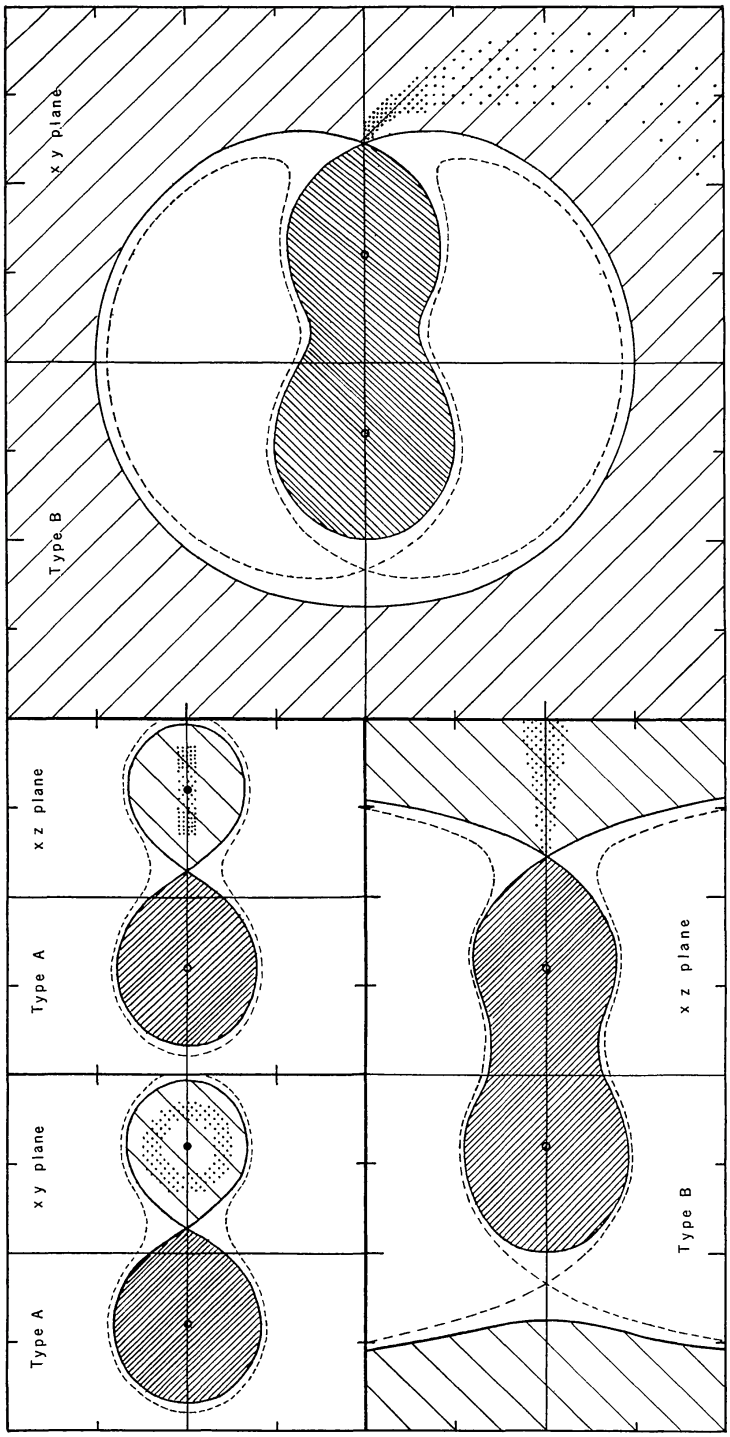

FIG. 5.—Surfaces of zero velocity and permitted regions (light shade) for ejection of types A and B. Small dots indicate actual positions of ejected particles. Stellar bodies are heavily shaded.

reduce in size, as is easily seen by multiplying, in equations (31)–(33), μ by $(1-\alpha)$ but leaving $(1-\mu)$ unchanged. Different results are obtained, however, if the ring should possess a considerable optical thickness in ultraviolet light, so that the stream falling toward the ring should experience little or no radiation pressure. Finally, the collisions active in rounding off the orbits will, if inelastic, tend to diminish the final radius.

Corresponding remarks may be made about ejection of type B. We see from Figure 5 that the ejected material cannot possibly form a *shell* around β Lyrae, as has often been assumed. The permitted region is shaded in Figure 5; but which part of this region is actually occupied can be found only from the equations of motion. If the velocity of ejection has a small z-component, the motion will be close to the xy-plane. It would again be possible to estimate the radius a of the ultimate orbit, by deriving the periodic orbit around the binary having the appropriate Jacobian constant,[44] if this periodic orbit were so stable that even the boundary conditions of the ejected particles would lead to an orbit not very different from the periodic orbit. This, however, is not the case, as will be seen later.

Further details about the orbits of the ejected particles can be obtained only by integration of equations (28). These equations being of the sixth order, the integration cannot be performed analytically except for small regions of space, where a first-order theory of small co-ordinate differences may be used. We shall therefore subdivide the discussion of equations (28) into two parts: (1) the motion near the points of ejection and (2) the motion farther away from these points. The first discussion can start from the standard theory of the motion near the Lagrangian points L_1 and L_2 (the unstable straight-line solutions); the second has to use numerical integrations.

5. THE MOTION NEAR THE POINTS OF EJECTION

The purpose of this section is to express the co-ordinates of the ejected material in terms of the initial conditions. Collisions and radiation pressure will be neglected; their effects are examined separately. The equations of motion are therefore equations (28). As initial conditions we assume that at $t = 0$ the particle has the co-ordinates of the libration point (L or G of Fig. 3) and the velocity components v_x, v_y, and v_z. We shall keep the mass ratio arbitrary except in the numerical work, where we shall use $M_A/M_B = 1.5$ (or $\mu = 0.4$). The discussion will be made to apply to ejection of either type A or type B. We shall use the same symbols as used in Moulton's textbook[45] and derive only such formulae as are not given there.[46]

If x', y', and z' are the co-ordinate differences in the rotating frame with respect to L or G and if these differences remain small ($\ll 0.1$), the motion in z' is periodic and is found to be

$$z = z' = \frac{v_z}{\sqrt{A}} \sin \sqrt{A}\, t\,. \tag{34}$$

The numerical values of A and other constants are found in Table 5 for both G and L; the period of the motion in z is $2\pi/\sqrt{A}$; its value, 4.77, for L, should be compared with 2π for the binary.

[44] The radius of the periodic orbit around AB, corresponding to $v_0 = 0$, is about 2.4; the radius is smaller for positive v_0.

[45] *Op. cit.*

[46] A review of the literature shows a vast amount of work carried out on the *problème restreint*, but few results are applicable to our problem which are not already contained in Moulton's book. The reason is that most of the numerical work (by G. H. Darwin, Thiele, Burrau, E. Strömgren, *et al.*) was done in search for periodic orbits, to which group the orbits discussed here do not belong.

The solutions for x' and y' are

$$x' = \sum_{1}^{4} K_j e^{\lambda_j t} ; \qquad y' = \sum_{1}^{4} L_j e^{\lambda_j t} , \tag{35}$$

in which the λ_j are the four roots of the equation

$$\lambda^2 = \frac{A - 2}{2} \pm \sqrt{2\tfrac{1}{4}A^2 - 2A} . \tag{36}$$

The values of A are such that the term under the square root in equation (36) is positive and that the values of λ^2 have opposite signs; the roots of equation (36) are, therefore, λ_1, $-\lambda_1$, $+i\sigma$, and $-i\sigma$, in which λ_1 and σ are positive, real numbers. Their values are given in Table 5.

TABLE 5

EJECTION CONSTANTS FOR $\mu = 0.4$

Constant	G (Type A)	L (Type B)	Constant	G (Type A)	L (Type B)
x	0.14162	1.2308	$-c_1 = +c_2$	0.3568	1.0748
A	7.92936	1.7320	c	4.3716	2.2973
z-period	2.2313	4.7742			
			h	0.089226	0.5516
λ_1	3.7646	1.2957	k	0.25007	0.5133
σ	2.8710	1.3953	l	0.020410	0.2401

The relation between the coefficients L_j and K_j, found by the introduction of equation (35) into the equations of motion, is

$$L_j = \frac{\lambda_j^2 - (1 + 2A)}{2\lambda_j} K_j = c_j K_j . \tag{37}$$

The constants c_j are also given in Table 5; $c_3 = -c_4$, is imaginary, $= ci$. If we now put

$$\left.\begin{aligned} K_1 + K_2 &= m ; & K_3 + K_4 &= n ; \\ K_1 - K_2 &= p ; & (K_3 - K_4)i &= q , \end{aligned}\right\} \tag{38}$$

we find, upon substitution of the boundary conditions in equation (35),

$$\left.\begin{aligned} 0 &= m + n ; & v_x &= \lambda_1 p + \sigma q ; \\ 0 &= -c_2 p + c q ; & v_y &= -c_2\lambda_1 m - c\sigma n . \end{aligned}\right\} \tag{39}$$

The solution is

$$\left.\begin{aligned} m = -n = h v_y, \qquad \text{in which} \qquad & h = \frac{1}{c\sigma - c_2\lambda_1} = \frac{2}{\lambda_1^2 + \sigma^2} , \\ p = k v_x \qquad\qquad\quad & k = \frac{c}{c\lambda_1 + c_2\sigma} = \frac{h}{c_2} , \\ q = l v_x \qquad\qquad\quad & l = \frac{c_2}{c\lambda_1 + c_2\sigma} = \frac{h}{c} . \end{aligned}\right\} \tag{40}$$

The numerical values of h, k, and l are found in Table 5. Equation (35) now becomes

$$\left.\begin{aligned} x' &= +m\cosh\lambda_1 t + p\sinh\lambda_1 t - m\cos\sigma t + q\sin\sigma t\,, \\ y' &= -c_2 m\sinh\lambda_1 t - c_2 p\cosh\lambda_1 t + cm\sin\sigma t + cq\cos\sigma t\,. \end{aligned}\right\} \tag{41}$$

It is noted that equation (41) is homogeneous in the initial velocity components and that the constants of Table 5 are all positive. For small t-values equation (41) reduces to a simple form due to certain relations between the different constants. Series development gives, up to the fourth order of t,

$$\left.\begin{aligned} x' &= v_x t + v_y t^2 + \frac{2A-3}{6} v_x t^3 + \frac{A-2}{12} v_y t^4 + \dots\,, \\ y' &= v_y t - v_x t^2 - \frac{A+3}{6} v_y t^3 - \frac{A-2}{12} v_x t^4 + \dots\,. \end{aligned}\right\} \tag{42}$$

Equation (42) gives fair accuracy for point L if $t < 1$ and for G if $t < \frac{1}{3}$. Considering only terms up to the second order, we find that, if the ejection takes place with a definite initial velocity, $v_0 = \sqrt{v_x^2 + v_y^2}$, but under all possible angles α, the trajectories are parabolae, equal in shape but of different orientation. They resemble the effect created by a pinwheel (cf. Fig. 6).

We return now to the case where t is not restricted. Again assuming v_0 to be constant but α arbitrary, we have

$$v_x = v_0\cos\alpha\,; \qquad v_y = v_0\sin\alpha\,, \tag{43}$$

and by equation (41)

$$\left.\begin{aligned} \frac{x'}{v_0} &= B\sin\alpha + C\cos\alpha \\ \frac{y'}{v_0} &= -D\sin\alpha - B\cos\alpha \end{aligned}\right\} \tag{44}$$

$$\text{if} \quad \left\{\begin{aligned} B &= h(\cosh\lambda_1 t - \cos\sigma t) \\ C &= h\left(\frac{1}{c_2}\sinh\lambda_1 t + \frac{1}{c}\sin\sigma t\right) \\ D &= h(c_2\sinh\lambda_1 t - c\sin\sigma t) \end{aligned}\right\} \tag{45}$$

The quantities B, C, and D depend on constants (which, in turn, depend on the libration point selected and on μ) and on the time. Table 6 gives their values for point L and the interval $1 \leqslant t \leqslant 3$, which, together with equation (42), covers the range needed. With B, C, and D known, equation (44) gives the position of the ejected particle for any α. The structure of equation (44) proves at once the following theorem: *The locus of the particles ejected simultaneously with the same velocity, v_0, but in all possible directions, α, is an ellipse centered on the point of ejection; the scale of the ellipse at a given time is proportional to v_0; and the orientation of the ellipse changes with time.*

The theorem is here stated in its two-dimensional form. Since the motion in the z-coordinate and that in x and y are independent, the theorem also holds if v_0 means the projection of the velocity of ejection on the xy-plane. In either case the validity is restricted to the region around the point of ejection (within 0.1 from L).

The equation of the locus is found by eliminating α from equation (44):

$$x^2(B^2 + D^2) + y^2(B^2 + C^2) + 2xyB(C + D) = (B^2 - CD)^2\,. \tag{46}$$

The direction of the principal axes of this ellipse is found from

$$\tan 2\varphi = \frac{2B}{D - C}\,; \tag{47}$$

and their lengths, a_1 and a_2, from

$$a_{1,2}^2 = 2(B^2 - CD)^2 \left\{ 2B^2 + C^2 + D^2 \mp (C + D)\sqrt{(D - C)^2 + 4B^2} \right\}^{-1}. \tag{48}$$

The value of φ lying in the fourth quadrant is found in Table 6.

Figure 6 shows the orbits of particles ejected from L in various directions α; all multiples of 45° are shown, and the more important multiples of 15° as well. It follows from

TABLE 6

CONSTANTS FOR L IF μ=0.4

t	B	C	D	φ
1.0	+ 0.987	+ 1.100	− 0.247	−27° 51′
1.2	+ 1.419	+ 1.393	+ 0.079	−32 35
1.4	+ 1.938	+ 1.744	+ 0.590	−36 43
1.6	+ 2.559	+ 2.179	+ 1.313	−40 12
1.8	+ 3.30	+ 2.73	+ 2.27	−42 59
2.0	+ 4.20	+ 3.45	+ 3.48	−45 08
2.2	+ 5.30	+ 4.38	+ 5.00	−46 40
2.4	+ 6.68	+ 5.60	+ 6.86	−47 41
2.6	+ 8.42	+ 7.20	+ 9.14	−48 17
2.8	+10.66	+ 9.22	+11.95	−48 39
3.0	+13.55	+11.90	+15.43	−48 43

equation (44) that if v_0 is chosen as unit, one such diagram is sufficient; the validity of Figure 6 is limited only by the condition $\sqrt{x^2 + y^2} \ll 0.1$. Hence, if $v_0 = 0.01$ (or 4.6 km/sec for β Lyrae) the whole of Figure 6 will be valid; but if $v_0 = 0.1$, only the vicinity of the origin will be valid.

Some orbits will be physically impossible, either partly or wholly, because of interference by the body of the star. The boundary of the star near the point of ejection is found from equation (5); putting $x = L + x'$, $y = y'$, we find for the xy-plane up to the second order in x' and y':

$$-\Omega = -\Omega_L + \frac{2A + 1}{2} x'^2 - \frac{A - 1}{2} y'^2\,. \tag{49}$$

This is valid for either L or G (cf. Fig. 3). If we now put $\Omega = \Omega_L$, we find for the boundary of the star two straight lines through L (or G):

$$\left.\begin{aligned} y' = \pm \sqrt{\frac{2A + 1}{A - 1}}\, x' &= \pm 2.469x' \quad \text{for} \quad L \\ &= \pm 1.559x' \quad \text{for} \quad G\,. \end{aligned}\right\} \tag{50}$$

A higher approximation than equation (50) can be made only if the unit v_0 is specified numerically.

It is of interest to derive from equation (49) the equipotential curve equivalent to the "curve of zero velocity" specified by v_0. From equations (29) and (5) we find the Jacobian constant C by

$$\tfrac{1}{2}v_0^2 + C = -\Omega_L .$$

Hence, for any point

$$\tfrac{1}{2}v^2 = -\Omega - C = -\Omega + \Omega_L + \tfrac{1}{2}v_0^2 .$$

The curve of zero velocity in the xy-plane is therefore, by equation (49),

$$\frac{2A+1}{2}\,x'^2 - \frac{A-1}{2}\,y'^2 + \tfrac{1}{2}v_0^2 = 0 . \tag{51}$$

This is a hyperbola of fixed dimensions if x'/v_0 and y'/v_0 are used as co-ordinates, as in the case in Figure 6; the asymptotes are given by equation (50). Again, in a higher approximation the curve of zero velocity would depend on v_0.

The full-drawn orbits in Figure 6 are physically possible; they lie outside the star. Particles ejected in directions $\alpha = -45°$ and $-90°$ are seen to fall back into the star. Physically impossible orbits are indicated by broken lines. The heavy dots on the possible orbits are spaced by 0.2 in t; they show how the velocity varies along the path (in the rotating frame). Furthermore, the surface density of these dots (except near the origin where obviously some dots have been omitted) is proportional to the *density of matter* in the xy-plane.

The ellipses (eq. [46]) are also shown; the parts of physical interest are full-drawn, the other parts broken. It is interesting to note how these ellipses avoid crossing the curve of zero velocity.

Figure 6 suggests that the orbits emanating from the origin tend to become straight lines, either in the second or in the fourth quadrant.[47] From equation (41) it follows that for large values of t

$$x' \cong \tfrac{1}{2}(m+p)\cdot e^{\lambda_1 t} ; \qquad \text{and} \qquad y' \cong -\tfrac{1}{2}c_2(m+p)\cdot e^{\lambda_1 t} , \tag{52}$$

so that the motion tends toward the straight line

$$y' = -c_2 x' . \tag{53}$$

Whether the asymptote is in the second quadrant or in the fourth appears to depend on the sign of $(m+p)$ or of the constant K_1 of (35). The limiting case, $(m+p) = K_1 = 0$, has curious properties. From equation (41) we then find, for any value of t,

$$\left.\begin{aligned} x' - me^{-\lambda_1 t} &= \sqrt{m^2+q^2}\,\sin(\sigma t - \psi) \\ y' - mc_2 e^{-\lambda_1 t} &= c\sqrt{m^2+q^2}\,\cos(\sigma t - \psi) \end{aligned}\right\}, \quad \text{if} \quad \left\{\begin{aligned} \frac{m}{\sqrt{m^2+q^2}} &= \sin\psi \\ \frac{q}{\sqrt{m^2+q^2}} &= \cos\psi \end{aligned}\right\}. \tag{54}$$

The right-hand side shows motion in an ellipse with eccentricity $e^2 = (c^2-1)/c^2$, having the major axis parallel to the y'-axis. These ellipses correspond to the well-known class of

[47] Cf. also S. S. Hough, in G. H. Darwin, *Scientific Papers*, 4, 118 ff., 1911

(unstable) periodic orbits around the libration points L_1, L_2, and L_3.[48] The curious fact is that the particle describes this orbit around a *displaced* center, given by the left-hand member of equation (54); the center of the orbit approaches the libration point asymptotically. The motion being *around* L or G, this limiting case, $(m + p) = 0$, is of no importance to the problem of ejection.

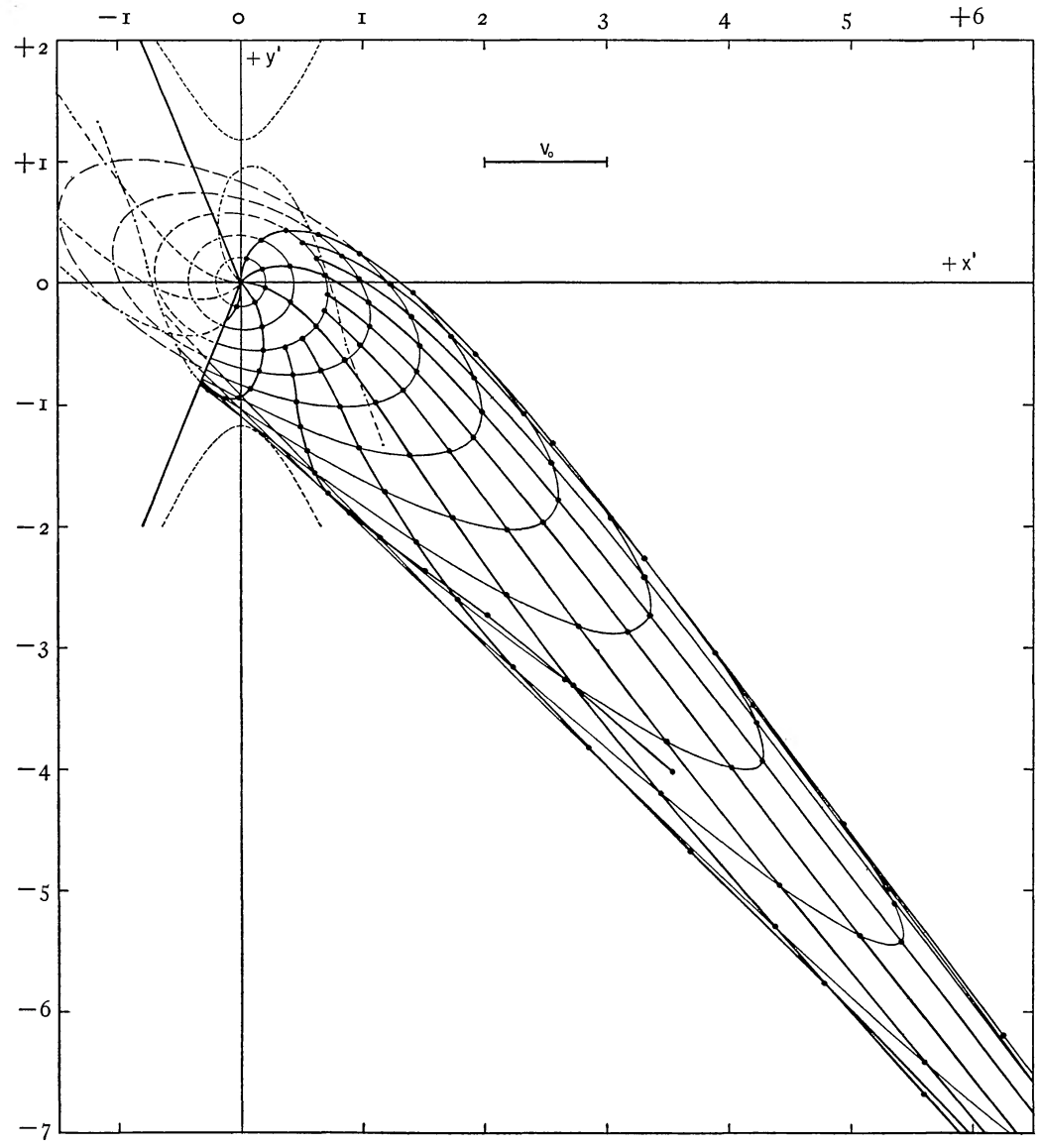

FIG. 6.—Ejection of type B in first-order theory; $\mu = 0.4$

For point L and $\mu = 0.4$ the values of α corresponding to this limiting case are $-42°.94$ and $+137°.06$. The latter value is of no practical importance, since it is inside the star. This shows that only material ejected between

$$-42°.94 < \alpha < +112°.05 \qquad (55)$$

[48] Moulton, *op. cit.*, p. 304.

will leave the star permanently; the upper limit corresponds to the slope of the boundary of the star according to equation (50).

The previous discussion applies to ejection from point G as well as from point L if for each case the appropriate constants from Table 5 are used. It will therefore be sufficient to reproduce the result of the computations in Figure 7. The dots are here only 0.1 apart in t, against 0.2 in Figure 6. It is noted that the higher-order terms of equation (42) begin to become important much sooner than in Figure 6, so that the pinwheel effect has almost disappeared. Figure 7 may be taken to show orbits emanating from the more massive star toward the less massive star, or vice versa, the diagram being point-symmetrical in the first-order theory.

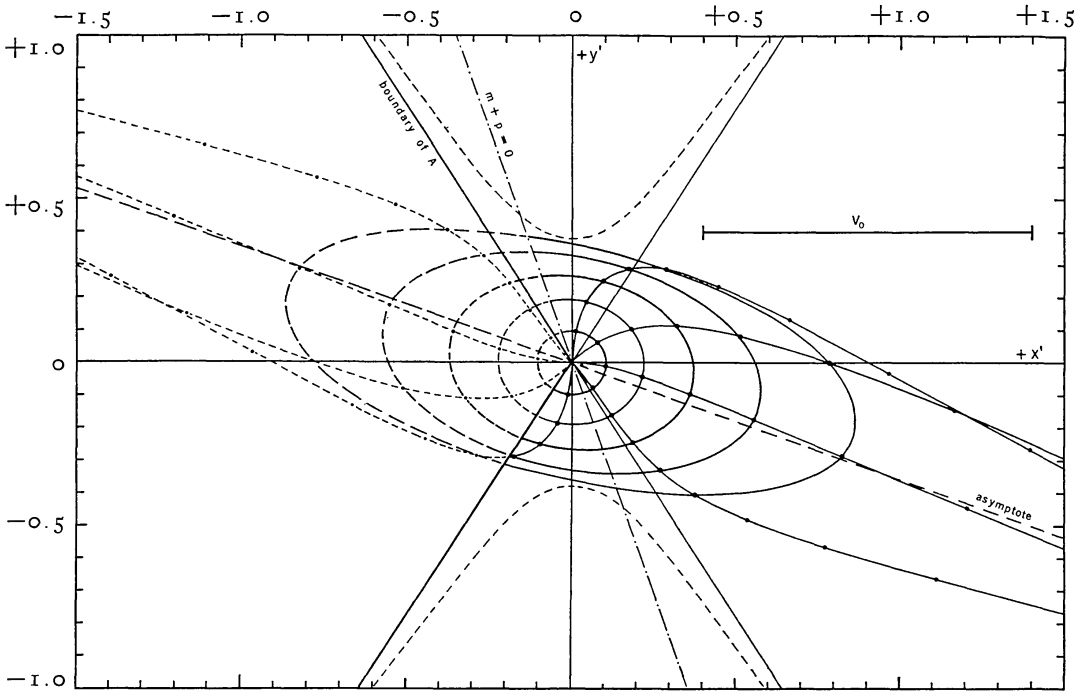

FIG 7.—Ejection of type A in first-order theory; $\mu=0.4$

The geometry of Figure 7 is such that all particles ejected in a whole hemisphere will leave the star permanently; the line of demarcation in the xy-plane, given as before by $(m + p) = 0$, is $109^\circ.64 \pm 180^\circ$.

Figures 6 and 7 show that for a given velocity of ejection, but for any value of a, the orbits of physical interest are quite similar for $t \gg 1$. But even the velocities at any point (x', y') of the common asymptotic orbit are the same, independently of v_0; for from equation (52) we find

$$\frac{dx'}{dt} = \lambda_1 x' \; ; \qquad \frac{dy'}{dt} = \lambda_1 y' \; , \tag{56}$$

in which λ_1 depends on the libration point and the mass ratio but not on v_0. In the frame of the first-order theory, therefore, *the motion of the ejected material is independent of the velocity and the angle of ejection except near the point of ejection itself.*

In the exact theory this invariance will be preserved *if* v_0 *is very small*, for then the motion of the ejected particle has already approached the asymptotic properties at the

time it leaves the region where the first-order theory applies. Figure 6 shows that this requires $v_0 \ll 0.01$.

This completes the discussion of the motion of the ejected material for the vicinity of the ejection points. Its application is the wider, the smaller the velocity of ejection is in terms of the relative orbital motion of the two stars. In the next two sections we trace the further course of the ejected matter by means of numerical integrations.

6. EJECTION OF TYPE A: ORBITS

The equations of motion are given by equation (28); we use, as before, $\mu = 0.4$. If $z \neq 0$, the acceleration $\ddot{z}$ will be of opposite sign to z; hence, excluding the improbable case of large initial $\dot{z}$, the values of z will always be small. The extension in the z-direction will probably be largely due to a pressure gradient in the accumulated gaseous body and is therefore not determined by equation (28). For these reasons we shall consider the plane problem based on equation (28).

The numerical integrations in this section and the next were carried out by using Taylor's formula up to the third derivative. If the time interval be δ, we have for x (and similarly for y)

$$\left.\begin{aligned} x(t+\delta) &= x(t) + \delta \cdot \dot{x}(t) + \frac{\delta^2}{2}\ddot{x}(t) + \frac{\delta^2}{6}\Delta\,, \\ \dot{x}(t+\delta) &= \dot{x}(t) + \delta \cdot \ddot{x}(t) + \frac{\delta}{2}\Delta\,, \end{aligned}\right\} \tag{57}$$

in which the third derivative is replaced by Δ/δ, and $\Delta = \ddot{x}(t+\delta) - \ddot{x}(t)$. At the boundary $x(t)$ and $\dot{x}(t)$ are given, and $\ddot{x}(t)$ is found from equation (28). The difference Δ has to be found from extrapolation once the integration is under way; if the value found in this way afterward appears to be too much in error, a new set of values for $x, \dot{x}, y, \dot{y}, r_1$, and r_2 has to be computed.

As each orbit requires several thousand numerical operations and as errors are cumulative, much work was carried out in duplicate, and numerous checks were made. All computations were made by the writer. A very useful check is found in Jacobi's constant (C of eq. [29]), the computation of which requires little additional work. Its deviations from constancy will not only reveal appreciable errors but will also show whether the series (57) is adequate.

Two orbits starting from the first libration point were computed, assuming $v_0 = 0.1$ and 0.5, respectively, the direction being along the positive x-axis in both cases. The results are found in Tables 7 and 8 and are shown in Figure 8. The interval δ was first taken as 0.1; but at $t = 0.7$ in Table 7 and at 0.3 in Table 8 the approximation (57) becomes too poor, as shown by the decrease in C, and smaller steps had to be taken. From then on, 0.01 was used, although not all steps are reproduced in the tables. The accuracy used in computing the increments, here as in the next section, was the nearest 0.00005 in x and y, 0.0001 in $\dot{x}$ and $\dot{y}$, and 0.001 or 0.01 in $\ddot{x}$ and $\ddot{y}$; but cumulative errors a few times larger than these values may be present apart from an error discussed below.

Near $t = 0.90$ (Table 7) and 0.49 (Table 8) a serious rise in C is noted which later practically disappears. This is due to the large arcs (up to 48°) covered in one step during the approach to B. The omission of the fourth derivative in equation (57) causes an error in the increment of x which is $\delta/4$ times that in $\dot{x}$; this ratio is 1/400 if $\delta = 0.01$. This shows that the change in C is almost entirely due to errors in the velocities. The co-ordinates would be affected appreciably only after several additional steps, whereas actually for only a few steps v is in error. Tables 7 and 8 show, in connection with the values of $\frac{1}{2}v^2$, also given, that the maximum errors in v are 4.3 and 2.0 per cent, respectively.

TABLE 7

t	x	y	$\dot{x}$	$\dot{y}$	$\frac{1}{2}v^2$	C
0.00	0.1416	0.0000	+0.100	0.000	0.005	1.986
.10	.1518	− .0010	+0.106	−0.020	0.006	1.986
.20	.1633	− .0041	+0.127	−0.042	0.009	1.985
.30	.1778	− .0095	+0.166	−0.066	0.016	1.985
.40	.1973	− .0175	+0.230	−0.095	0.031	1.985
.50	.2250	− .0287	+0.332	−0.131	0.064	1.985
.60	.2657	− .0441	+0.497	−0.176	0.139	1.982
.70	.3286	− .0639	+0.790	−0.219	0.336	1.975
.72	.3452	− .0683	+0.871	−0.225	0.405	1.974
.74	.3635	− .0728	+0.966	−0.227	0.493	1.974
.76	.3839	− .0773	+1.079	−0.223	0.607	1.975
.78	.4068	− .0814	+1.214	−0.208	0.759	1.975
.80	.4327	− .0854	+1.381	−0.174	0.969	1.974
.82	.4623	− .0882	+1.594	−0.104	1.275	1.974
.84	.4968	− .0890	+1.874	+0.042	1.756	1.972
.85	.5164	− .0880	+2.049	+0.172	2.114	1.973
.86	.5379	− .0854	+2.252	+0.372	2.605	1.971
.87	.5616	− .0801	+2.477	+0.698	3.311	1.971
.88	.5874	− .0706	+2.674	+1.258	4.366	1.994
.89	.6142	− .0536	+2.611	+2.216	5.864	2.124
.90	.6368	− .0257	+1.684	+3.376	7.116	2.594
.91	.6455	+ .0111	+0.045	+3.716	6.906	2.441
.92	.6391	+ .0454	−1.144	+3.087	5.418	2.042
.93	.6252	+ .0725	−1.564	+2.370	4.031	1.966
0.94	0.6089	+0.0935	−1.654	+1.856	3.090	1.952

TABLE 8

t	x	y	$\dot{x}$	$\dot{y}$	$\frac{1}{2}v^2$	C
0.00	0.1416	0.0000	+0.500	0.000	0.125	1.866
.10	.1929	− .0051	+0.535	−0.102	0.148	1.865
.20	.2515	− .0205	+0.655	−0.208	0.236	1.862
.30	.3290	− .0465	+0.930	−0.309	0.480	1.851
.32	.3484	− .0528	+1.013	−0.326	0.567	1.850
.34	.3697	− .0594	+1.114	−0.338	0.678	1.851
.36	.3931	− .0663	+1.237	−0.342	0.824	1.850
.38	.4193	− .0730	+1.391	−0.330	1.022	1.850
.40	.4490	− .0793	+1.588	−0.288	1.303	1.850
.42	.4833	− .0842	+1.849	−0.184	1.726	1.850
.44	.5236	− .0858	+2.200	+0.062	2.421	1.850
.45	.5466	− .0840	+2.411	+0.301	2.952	1.852
.46	.5718	− .0792	+2.623	+0.690	3.678	1.860
.47	.5988	− .0694	+2.745	+1.312	4.627	1.912
.48	.6256	− .0520	+2.524	+2.206	5.619	2.059
.49	.6473	− .0256	+1.701	+3.028	6.031	2.192
.50	.6586	+ .0066	+0.583	+3.272	5.523	2.041
.51	.6598	+ .0381	−0.259	+2.992	4.508	1.911
.52	.6547	+ .0660	−0.710	+2.579	3.577	1.875
.53	.6464	+ .0899	−0.925	+2.212	2.875	1.864
0.54	0.6366	+0.1105	−1.018	+1.919	2.359	1.862

The velocities in the rotating frame, $\dot{x}$ and $\dot{y}$, are added in Tables 7 and 8 because of their astrophysical importance. If X and Y are the velocities in a stationary frame having, at the moment considered, the same orientation as the rotating frame, we find X and Y from

$$X = \dot{x} - y\,; \qquad Y = \dot{y} + x\,. \tag{58}$$

These values determine the Doppler shifts of absorption and emission lines. (The unit of velocity is the relative velocity of A and B.)

As anticipated by the discussion of Figure 7, the orbits in Figure 8 are quite similar, and no further integrations seem necessary. The motion around B is direct, as was assumed in section 4 in the derivation of the radius of the ultimate mean orbit of the ejected gas.

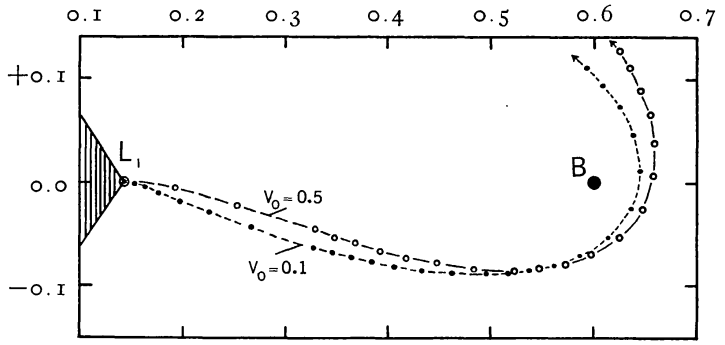

FIG. 8.—Orbits for ejection of type A; μ=0.4. Dots not equally spaced in time; they correspond to Tables 7 and 8.

The integrations may be easily extended to include radiation pressure by a hot component, B. We multiply in equation (28) the mass μ by $(1 - \alpha)$ but leave $(1 - \mu)$ unchanged. The Coriolis force ($2\dot{y}$ or $-2\dot{x}$) remains the same, of course, and also the terms x and y, because the period of the binary is not affected by the radiation pressure. Because of varying optical thickness $(1 - \alpha)$ will vary with position.

7. EJECTION OF TYPE B: ORBITS

We shall first investigate the fate of a stream of gas assumed to be parallel at some initial point near a of Figure 4, a, passing over the surface of B without friction. Struve found such a stream in β Lyrae having a velocity of about 300 km/sec. We shall adopt $v_0 = 0.55$, which corresponds to 250 km/sec for β Lyrae, if $M_A/M_B = 1.5$. This somewhat smaller value was chosen to compensate in part for neglected viscous forces.

For the initial x-co-ordinate we adopt $x = 0.40$; and for the velocity components of the parallel stream $\dot{x} = +0.44$, and $\dot{y} = -0.33$ ($v_0 = 0.55$), which means that for $y = -0.30$ the stream is directed away from the center of gravity (F of Fig. 3). We have made integrations for three initial values of y: -0.30, -0.34, and -0.38. The orbits are found in Tables 9–11 and are illustrated in Figure 9: for brevity 15 lines were omitted in Table 11.

As in Tables 7 and 8, the Jacobian constant is added as a check of the numerical work and of the approximation (57). In one instance an experiment was made by integrating with larger steps (0.5) as well as with those used in the tables (0.1). In this case it was found that 0.12 of the error in C was due to errors in the co-ordinates, and 0.88 to the velocities, confirming the general remarks made on page 160.

Figure 9 shows that the interior part of the stream will tend to swing around the sec-

ondary, whereas the outer part will fly off into space. These results were anticipated on page 149. The inner orbits, as computed, intersect with the star; but in reality the matter will, of course, more or less follow the stellar surface, the pressure gradient near that surface having been neglected in the integrations.

Figure 9 also shows the surface of zero velocity corresponding to the middle orbit ($C = 1.690$), taken from section 3. It shows that for the high velocity adopted here the outlet of B is, indeed, wide open. It would clarify the picture if additional integrations were made for $-y = 0.35$, 0.36, 0.37, 0.39, and 0.40. These would also show the *width* of the tail to be expected.

TABLE 9

t	x	y	$\dot{x}$	$\dot{y}$	$\frac{1}{2}v^2$	C
0.0.....	+0.4000	−0.3000	+0.440	−0.330	0.151	1.785
.1.....	+ .4475	− .3246	+ .512	−0.160	.144	1.785
.2.....	+ .5027	− .3317	+ .594	+0.021	.177	1.785
.3.....	+ .5666	− .3193	+ .683	+0.234	.260	1.786
.4.....	+ .6386	− .2827	+ .752	+0.513	.414	1.789
.5.....	+ .7134	− .2132	+ .719	+0.898	.662	1.800
0.6.....	+0.7720	−0.1013	+0.379	+1.337	0.966	1.850

TABLE 10

t	x	y	$\dot{x}$	$\dot{y}$	$\frac{1}{2}v^2$	C
0.0.....	+0.4000	−0.3400	+0.440	−0.330	0.151	1.691
0.1.....	+ .4457	− .3665	+ .475	−0.200	.132	1.691
0.2.....	+ .4952	− .3800	+ .516	−0.069	.136	1.691
0.3.....	+ .5492	− .3801	+ .565	+0.067	.162	1.691
0.4.....	+ .6082	− .3662	+ .614	+0.215	.212	1.691
0.5.....	+ .6717	− .3365	+ .652	+0.383	.286	1.693
0.6.....	+ .7375	− .2888	+ .655	+0.575	.380	1.695
0.7.....	+ .8005	− .2212	+ .592	+0.777	.477	1.699
0.8.....	+ .8530	− .1346	+ .442	+0.942	.542	1.703
0.9.....	+ .8871	− .0358	+ .236	+1.012	.540	1.703
1.0.....	+ .9006	+ .0642	+ .044	+0.971	.472	1.698
1.1.....	+ .8980	+ .1560	− .082	+0.857	.370	1.693
1.2.....	+ .8864	+ .2348	− .149	+0.720	.270	1.689
1.3.....	+0.8707	+0.3001	−0.160	+0.587	0.185	1.689

The fact that we have neglected viscous forces may, however, have led to a velocity of ejection at the libration point L_2 which is too high. This velocity is about 0.53, or some 245 km/sec for β Lyrae. Obviously, a test is provided by the measured velocity of the B5 absorption spectrum, which is roughly −70 km/sec, or −50 km/sec with respect to the center of gravity. This value gives the radial component along the line passing through A, measured in a fixed frame of reference. Accordingly, we have to continue the integration of Table 11 indefinitely. Fortunately, if we surpass a point about three times the distance AB from the center of gravity, we may approximate the problem by a two-body problem, having unit mass in the origin and an infinitesimal mass moving outward, with initial co-ordinates and velocity components given by Table 11, last line. From equation (58) we find X and Y; the energy integral

$$v^2 = X^2 + Y^2 = \frac{2}{r} - \frac{1}{a} \tag{59}$$

will then show whether the subsequent motion will be in an ellipse ($a > 0$) or a hyperbola ($a < 0$).

From the last line of Table 11 we find $-1/a = 0.3140$, showing that the matter will move out in a hyperbola with $a = 3.184$. Furthermore, equation (59) shows that for large r the asymptotic velocity is 0.5604, or about 260 km/sec for β Lyrae. The velocity nearer to the system will, by equation (59), be even larger, although without computation it is not certain that this also applies to the component measured in the radial velocity. We shall show below that this is the case and that a smaller velocity of ejection at L_2 is required. This makes it very probable that *viscous forces are slowing down appreciably the current around* B.

TABLE 11

t	x	y	$\dot{x}$	$\dot{y}$	$\frac{1}{2}v^2$	C
0.0	+0.4000	−0.3800	+0.440	−0.330	0.151	1.610
0.2	+0.4899	−0.4267	+0.463	−0.140	0.117	1.610
0.4	+0.5864	−0.4369	+0.506	+0.036	0.128	1.610
0.6	+0.6924	−0.4128	+0.553	+0.203	0.173	1.611
0.8	+0.8055	−0.3568	+0.571	+0.352	0.225	1.612
1.0	+0.9174	−0.2760	+0.542	+0.440	0.244	1.612
1.2	+1.0213	−0.1880	+0.500	+0.420	0.214	1.611
1.4	+1.1200	−0.1145	+0.495	+0.301	0.168	1.611
1.6	+1.2218	−0.0715	+0.528	+0.121	0.146	1.611
1.8	+1.3319	−0.0683	+0.573	−0.093	0.168	1.611
2.0	+1.4498	−0.1104	+0.602	−0.330	0.236	1.612
2.2	+1.5703	−0.2017	+0.596	−0.584	0.348	1.612
2.4	+1.6847	−0.3445	+0.538	−0.845	0.502	1.612
2.6	+1.7816	−0.5393	+0.420	−1.101	0.695	1.613
2.8	+1.8484	−0.7839	+0.236	−1.340	0.926	1.613
3.0	+1.8717	−1.0731	−0.014	−1.545	1.193	1.613
3.1	+1.8630	−1.2319	−0.163	−1.629	1.340	1.614
3.2	+1.8386	−1.3984	−0.327	−1.698	1.495	1.614
3.3	+1.7972	−1.5710	−0.504	−1.751	1.659	1.614
3.4	+1.7375	−1.7479	−0.692	−1.784	1.831	1.615
3.5	+1.6584	−1.9271	−0.891	−1.797	2.012	1.615
3.6	+1.5590	−2.1065	−1.097	−1.788	2.200	1.615
3.7	+1.4387	−2.2838	−1.309	−1.754	2.396	1.616
3.8	+1.2970	−2.4565	−1.524	−1.696	2.600	1.616
3.9	+1.1340	−2.6222	−1.738	−1.613	2.811	1.617
4.0	+0.9496	−2.7783	−1.949	−1.503	3.030	1.617
4.1	+0.7443	−2.9221	−2.155	−1.368	3.256	1.617

Instead of computing the elements of the hyperbola from the focus at the origin and from x, y, $\dot{x}$, $\dot{y}$, and then computing an ephemeris, it was found simpler to continue the numerical integrations in a nonrotating frame by means of the equations

$$\ddot{x} = -\frac{x}{r^3}; \qquad \ddot{y} = -\frac{y}{r^3}, \tag{60}$$

the accelerations being small; the interval used in equation (57) was now 0.5. The results are shown in Figure 10 for a nonrotating frame and in Figure 11 for a rotating frame; Figure 11 extends Figure 9. The velocity vectors computed for a stationary frame are also shown. The projections along radii drawn from A appear to be only slightly less than the space velocities themselves, or about 300–400 km/sec for β Lyrae, a value much higher than that observed.

From the Jacobian constant computed for the last point, $t = 9.6$, we find that the two-body approximation has introduced an error in the velocity (or co-ordinates) well under 1 per cent.

We now turn to smaller velocities of ejection. In order to avoid difficulties arising from viscosity, we start the following integrations at L_2 (or L in Fig. 3). The following discussion therefore extends the theory given in section 5 to large distances from the libration point.

Two velocities were adopted: $v_0 = 0.1$ and 0.01. Together with the orbit of Table 11 ($v_0 = 0.53$) they should suffice to determine the order of magnitude of v_0 responsible for the measured radial velocity of the B5 spectrum of β Lyrae.

The results are given in Tables 12 and 13 and are shown in Figure 12. For brevity, Table 12 shows for $0.0 < t < 3.2$ only half the steps used in the integrations,

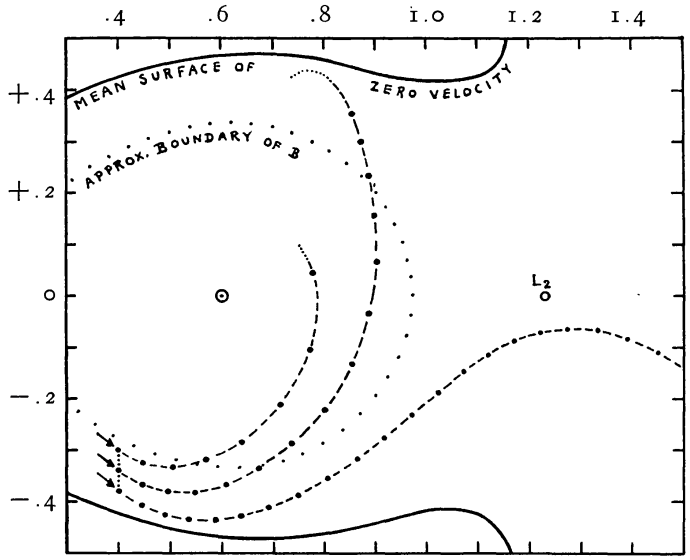

FIG. 9.—Orbits for ejection of type B; μ=0.4. Viscous forces neglected, and also presence of B's boundary.

and Table 13 shows only one-quarter. Since the amount of work done was already considerable, the integrations were not continued beyond the point where the radial-velocity test mentioned above could be applied.

The energy integral (eq. [59]) is valid only in the two-body problem; but we may test empirically the error made if we use equation (59) too close to the binary system. From the integration for $v_0 = 0.1$ we find the data of Table 14. In all three cases a positive value of $1/a$ is found, but the value has not yet reached its final value at $r < 3$. The asymptotic value for large r is probably still slightly above zero. The motion at $r \gg 3$ is therefore in a very long ellipse ($a \gg 100$) and, for practical purposes, in a parabola.

From the orbit with $v_0 = 0.01$ we find, at $t = 5.5$, that $r = 2.24$ and $1/a = -0.1275$. In view of the run of $1/a$ in Table 14 and the similarity between the two orbits, we may expect the true value of $1/a$ to be even somewhat smaller. Hence, the motion is in a hyperbola with $a < 7.8$; and $v_\infty > 0.357$, or >164 km/sec for β Lyrae.

We have found the curious result that for v_0 small ($\sim$0.01, or 5 km/sec for β Lyrae), as well as large ($\sim$0.5, or 250 km/sec for β Lyrae), the ejected matter will recede from the binary with a large hyperbolic velocity, but that at an intermediate velocity of ejection ($\sim$0.1 or 50 km/sec for β Lyrae) the matter moves out in a roughly parabolic or even elliptic orbit. This shows that the observed velocity of recession, about 50 km/sec, is

within the range covered by our mechanism. It would be of interest to have additional integrations for $v_0 = 0.05$ and 0.2 and also to investigate the effect of the angle α of ejection.

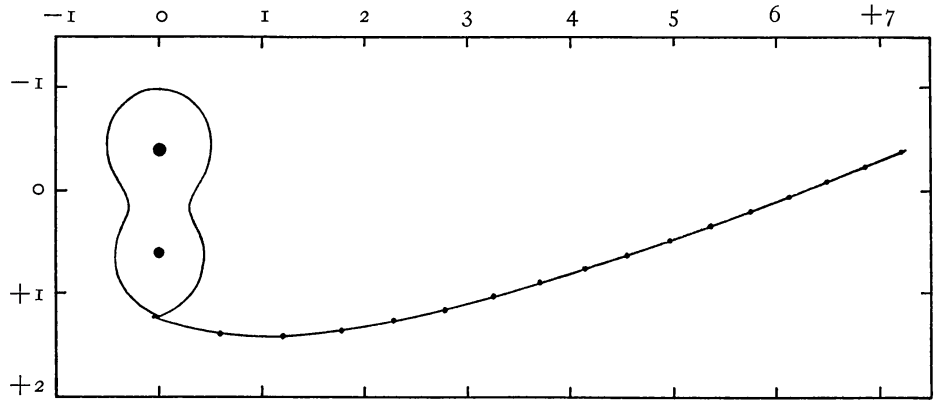

FIG. 10.—Ejection of type B; orbit in stationary frame. Position of binary given for moment of ejection. (Turned 90° with respect to other figures.)

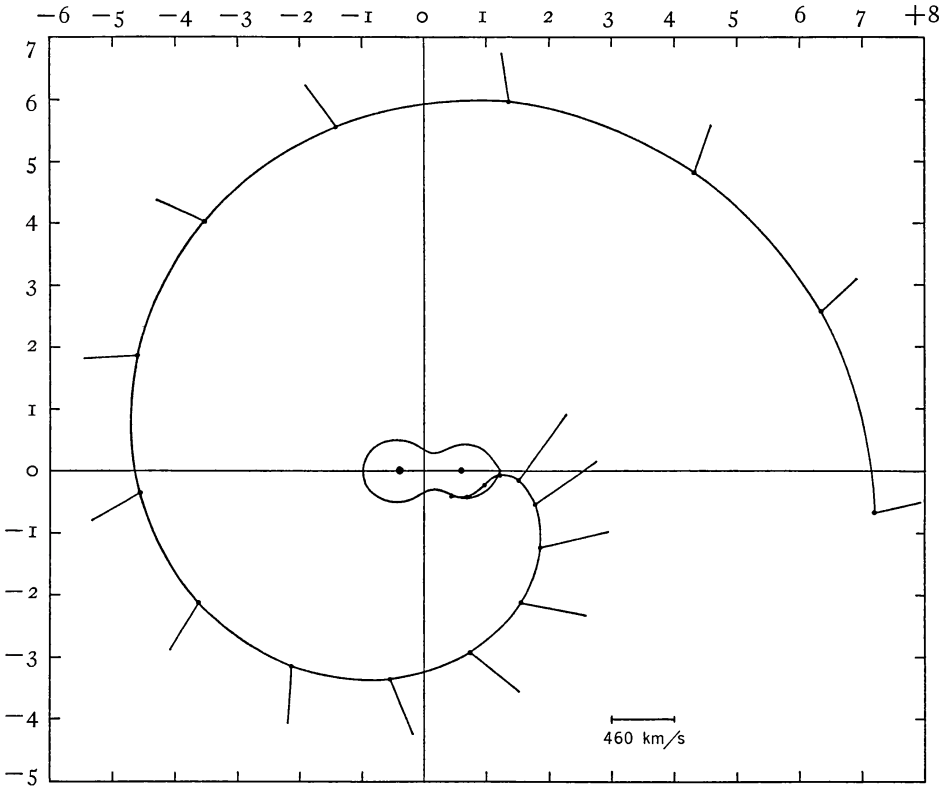

FIG. 11.—Extension of Fig. 9 for ejection orbit. Same orbit as in Fig. 10 but now in rotating frame. Dots are for $t = 0.1, \ldots, 9.6$, spaced by 0.5 (cf. Table 11). Velocity vectors, measured in a stationary frame, are indicated by short lines.

Radiation pressure may be introduced in the integration, as indicated earlier, but the complications due to eclipses and varying optical thickness will be serious. In view of the large velocities considered here, the effects of collisions on the x and y co-ordinates will

TABLE 12

t	x	y	$\dot{x}$	$\dot{y}$	$\frac{1}{2}v^2$	C
0.0	+1.2320	0.0000	+0.100	0.000	0.005	1.754
0.2	+1.2521	−0.0040	+0.101	−0.040	0.006	1.754
0.4	+1.2726	−0.0160	+0.104	−0.080	0.009	1.754
0.6	+1.2937	−0.0361	+0.107	−0.121	0.013	1.754
0.8	+1.3154	−0.0643	+0.110	−0.162	0.019	1.754
1.0	+1.3379	−0.1008	+0.114	−0.204	0.027	1.754
1.2	+1.3610	−0.1462	+0.117	−0.250	0.038	1.754
1.4	+1.3848	−0.2011	+0.120	−0.301	0.052	1.755
1.6	+1.4088	−0.2669	+0.120	−0.358	0.071	1.755
1.8	+1.4324	−0.3450	+0.115	−0.424	0.097	1.755
2.0	+1.4542	−0.4374	+0.102	−0.500	0.130	1.755
2.2	+1.4721	−0.5459	+0.076	−0.586	0.175	1.754
2.4	+1.4830	−0.6724	+0.031	−0.680	0.232	1.754
2.6	+1.4827	−0.8183	−0.037	−0.779	0.304	1.754
2.8	+1.4660	−0.9842	−0.134	−0.878	0.394	1.754
3.0	+1.4268	−1.1689	−0.263	−0.967	0.502	1.754
3.2	+1.3585	−1.3700	−0.426	−1.040	0.631	1.755
3.3	+1.3113	−1.4753	−0.519	−1.066	0.703	1.755
3.4	+1.2544	−1.5829	−0.620	−1.084	0.780	1.755
3.5	+1.1870	−1.6918	−0.729	−1.093	0.862	1.755
3.6	+1.1085	−1.8010	−0.843	−1.091	0.950	1.755
3.7	+1.0182	−1.9096	−0.963	−1.077	1.043	1.756
3.8	+0.9158	−2.0160	−1.087	−1.050	1.141	1.756
3.9	+0.8008	−2.1190	−1.213	−1.008	1.244	1.756
4.0	+0.6732	−2.2172	−1.341	−0.953	1.352	1.756
4.1	+0.5327	−2.3090	−1.468	−0.881	1.466	1.756
4.2	+0.3796	−2.3929	−1.593	−0.794	1.584	1.756
4.3	+0.2143	−2.4668	−1.713	−0.691	1.706	1.756
4.4	+0.0372	−2.5301	−1.828	−0.572	1.834	1.756
4.5	−0.1510	−2.5806	−1.934	−0.437	1.965	1.756
4.6	−0.3492	−2.6169	−2.030	−0.286	2.101	1.757
4.7	−0.5566	−2.6374	−2.114	−0.121	2.242	1.757
4.8	−0.7716	−2.6407	−2.184	+0.057	2.386	1.757
4.9	−0.9928	−2.6255	−2.238	+0.248	2.535	1.757

TABLE 13

t	x	y	$\dot{x}$	$\dot{y}$	$\frac{1}{2}v^2$	C
1.4*	+1.2494	−0.0194	−0.019	−0.028	0.001	1.760
1.8	+1.2588	−0.0326	+ .031	−0.042	0.001	1.760
2.2	+1.2738	−0.0523	+ .050	−0.064	0.003	1.760
2.6	+1.2975	−0.0831	+ .077	−0.102	0.008	1.759
3.0	+1.3331	−0.1327	+ .111	−0.166	0.020	1.759
3.4	+1.3833	−0.2129	+ .148	−0.267	0.047	1.760
3.8	+1.4467	−0.3408	+ .170	−0.419	0.102	1.760
4.2	+1.5127	−0.5381	+ .143	−0.628	0.208	1.761
4.6	+1.5548	−0.8265	+ .020	−0.881	0.388	1.761
5.0	+1.5276	−1.2172	− .248	−1.128	0.667	1.765
5.4	+1.3682	−1.6971	−0.683	−1.290	1.066	1.769

* The interval $0.0 < t < 1.4$ is obtained from the first-order theory in section 5.

probably be negligible except near the point of ejection itself. The effect on the z–co-ordinate will be to increase the vertical thickness of the tail over the dimensions determined by the z-velocities at the point of ejection.

8. APPLICATIONS

Applications to the problem of β Lyrae itself have been made throughout the paper. We may add that the asymmetrical light-curve (Fig. 1) can now be attributed to obscuration by the tail.

In section 5 we found the period for the motion in the z–co-ordinate to be 4.77, based on the first-order theory. If at the moment of ejection the amplitude is zero, the maximum amplitude will therefore be reached at $t = 1.19$; this is on the very edge where the first-order theory may be applied (cf. Table 12). This maximum semiamplitude according to equation (34) is $v_z/\sqrt{1.73}$. If v_z is of the order of the atomic velocities (about 0.01, compared to $v_0 = 0.1$), we find for the total extension in z only 0.015. This is small, compared to the dimension of the "outlet" of B as determined by the surface of zero velocity; for $v_0 = 0.1$ this dimension is about 0.2. We may therefore assume that the extension in z of the tail in the neighborhood of the binary is largely determined by the width of the outlet of B. This width is easily found from Jacobi's integral for any value of v_0.

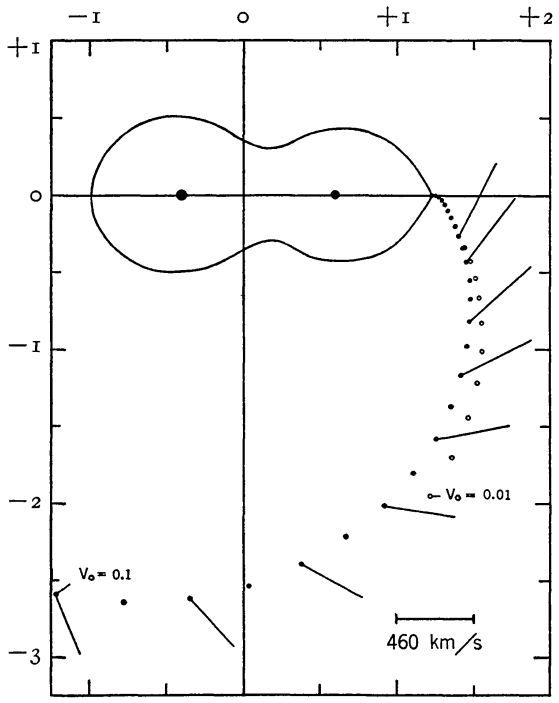

FIG. 12.—Ejection orbits of type B for v_0=0.1 and 0.01. Velocity vectors in stationary frame are indicated for v_0=0.1. Dots spaced 0.2 in t: cf. Tables 12 and 13.

The tail, therefore, does not cover the whole of A's disk when it emerges from eclipse after primary minimum but cuts out an equatorial strip roughly one-fifth of the diameter of the star. The rest of the disk is covered with the much more diluted gas of successive windings of the spiral which have acquired greater extension in z, owing to random initial velocities and to collisions.

The density measured per unit length along the tail (line density) falls off rapidly, as is seen from Tables 11–13 and from Figures 6, 11, and 12. The line density is obviously $\propto 1/v$, in which v is measured in the rotating frame. The space density falls off even more rapidly because of the increasing width of the tail in both co-ordinates perpendicular to its direction.

The gas streaming off from B must be comparatively cool, because (*a*) B is cool; (*b*) the region of ejection is the coolest part of B, gravity there being almost zero; (*c*) this region is eclipsed from radiation by A.

Some time after this cool gas has left B, it becomes exposed to radiation from A. If $v_0 = 0.1$, this happens between $t = 2.0$ and 2.5, or for β Lyrae between 4 and 5 days after ejection. It would be of interest to determine theoretically the time required for this gas to become mostly ionized by A. Without computation it may be said that the absorption lines of H and He I will be strong at first, if the B8 star is viewed through this cloud. This will account in part for the excessive strength of these lines shortly after

primary minimum, although other factors, mentioned below, enhance the effect. The spectral type, roughly B2–B5, must be a combined effect of the low density of matter and the somewhat diluted radiation by the B8 supergiant.

Proceeding along the first winding of the tail, we find (1) diminishing density—at first rapid, later more slowly; (2) increased extension in the z-direction; and (3) for the first 180° of the tail increasing ionization. Factors (1) and (3) will tend to diminish the strength of the absorption spectrum and (2) to increase it until the z-extension has reached the diameter of A. The observations show a pronounced decrease until after secondary minimum; then a slow increase takes place toward the next primary minimum. It seems possible that factor (3) reverses itself some time after secondary minimum, owing to the increasing distance from A and the fact that the side of A then visible may in part be covered by a cool returning current coming from B (cf. sec. 3).

At the completion of the first winding, the gas enters eclipse (cf. Fig. 11). The duration of this eclipse is of the order of a day, depending on v_0. The eclipse may well be

TABLE 14

t	r	$1/a$
3.5.....	2.067	+.0311
4.2.....	2.423	.0130
4.9.....	2.807	+.0078

total for the nearer windings. The effect will be a drop in the ionization; how much, only computation can show. This will result in a fresh absorption by the time the gas comes out of eclipse. At this time the z-extension is probably sufficient to cover most of A's disk; it is probable, therefore, that the effect of the second winding is even more important than the first one in producing a strong absorption after primary eclipse. Even the third and higher windings may have some effect, since the eclipse would affect them also.

There is an observational reason, as well, which suggests that the second and higher windings contribute considerably to the observed blend in absorption. The recessional velocity in the first quarter of the first winding is large, of the order of 0.6, or some 275 km/sec for β Lyrae. This value is much in excess of the observed 50 km/sec. It is true that we made integrations for only three values of v_0 (0.01, 0.1, and 0.53) and that a more favorable orbit could probably be found. But on dynamical grounds it seems certain that the recession of the first winding could not be brought below 200 km/sec (being about half the orbital velocity in the system AB). For the second and third windings the recessional velocity is much reduced, although perhaps not quite enough. If the ejection takes place in a highly elliptical orbit ($a \gg 10$), the velocity v is not much larger than the recessional velocity, as observed from A (cf. Fig. 9, drawn for hyperbolic motion). The latter being 50 km/sec, v could not exceed 100 km/sec at the distance r where the "mean" absorption takes place. The energy integral (59) gives, for $v = 0.2$ (92 km/sec) and for different a values, the following distances,[49] r:

a	r	a	r
10.....	14	100.....	40
20.....	22	∞.....	50
50.....	33		

[49] A more precise value of r giving dr/dt = 50 km/sec can be only found after the eccentricity or the parameter of the ellipse is specified. Our procedure underestimates r for large a.

This shows that the ejection has to be in a decidedly elliptical orbit in order that the mean distance shall not be excessive. Nevertheless it seems difficult to make the mean distance less than 10. This result is essentially due to the fact that β Lyrae is such a massive system and that orbital motion in its vicinity must be fast.

We conclude that the first winding is not of primary importance in producing the absorption spectrum, because the z-dimension of the tail is still insufficient to cover A's

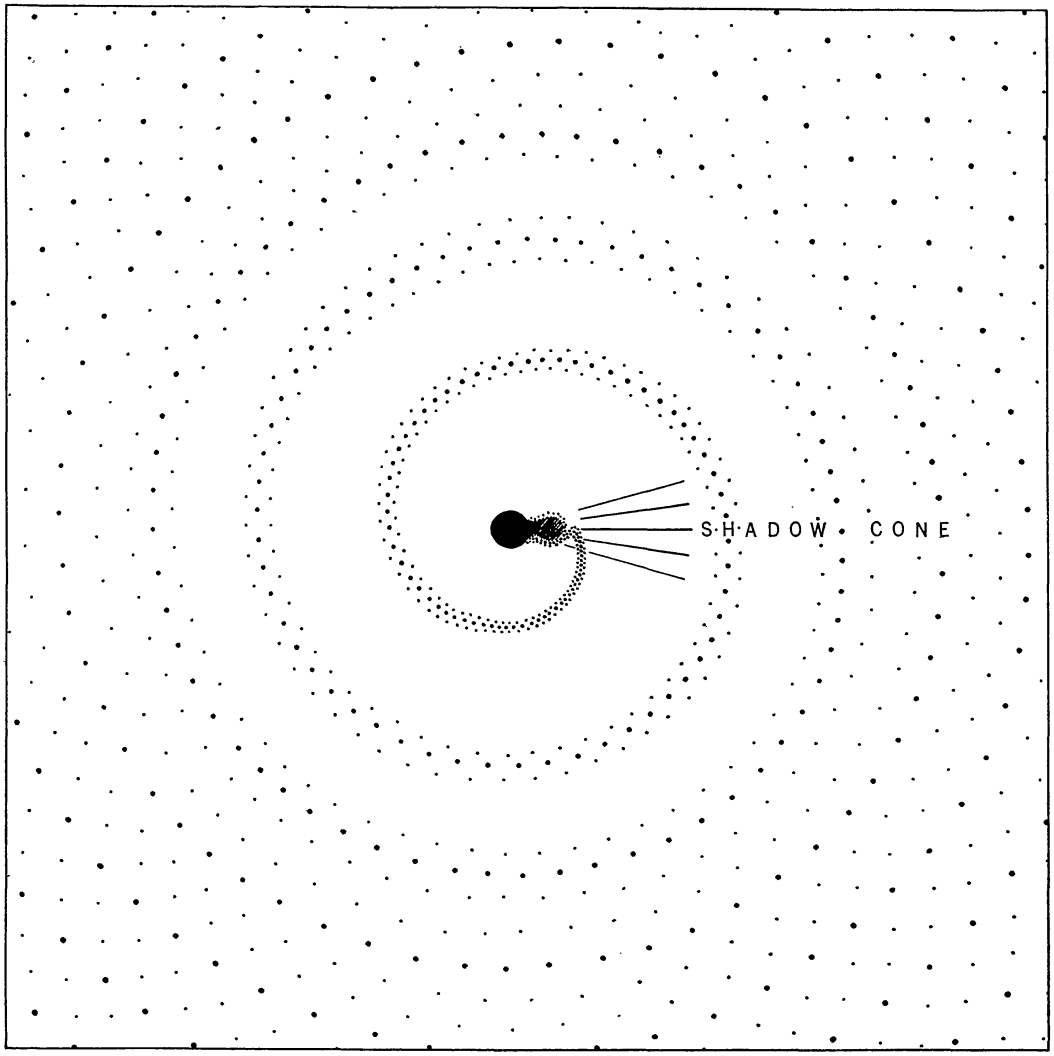

FIG. 13.—The system of β Lyrae in a frame rotating with the binary. Heavy dots indicate the central line of the spiral; light dots indicate schematically the width of the successive windings.

disk; that the next one or two windings are most effective in the absorption process; and that the still higher windings become of increasingly smaller importance. Further, the eclipse of the tail must play a major role in producing the fluctuations with phase of the line intensity. The picture developed is shown schematically in Figure 13. Since the ejection could not be perfectly regular, minor fluctuations in the line intensities and the radial velocities, as have been observed, should be expected. Finally, the inclination of the orbit must be quite close to 90° (within 2° or so).

The observed *emission* will obviously come from the whole visible part of the spiral,

with an intensity distribution depending on the density of matter and the degree of ionization. The problem is similar to that considered by B. Strömgren for interstellar matter surrounding hot stars.[50] The smoothness of the emission lines suggests that several windings of the spiral contribute to their formation. Their greatest width would be determined by the velocities of the inner winding; from Figure 12 we find about $2 \times 0.9 \times 460$ km/sec $\cong$ 800 km/sec, in good agreement with observation.

The irregularities in the light-curve at all phases are quite understandable on the basis of the picture developed.

One problem yet to be discussed is *the change in period of* β *Lyrae*. Various factors might be considered in this connection: (*a*) mass transfer from A to B, with constant total mass; (*b*) loss of mass and momentum by ejection of type B; (*c*) pressure at the interface between A and B.

Effect (*a*) was considered in section 2, with the result that a considerable *shortening* of the period should result from it.

The momentum per unit mass of the ejected matter is not constant as long as the three-body theory has to be applied; but as soon as the matter has receded far enough for the two-body approximation to become applicable, the momentum remains constant, because this constancy is identical with the validity of Kepler's law of areas. The momentum per unit mass of ejected gas may therefore be computed from the last line of Table 12, $v_0 = 0.1$ being the most probable ejection velocity obtained. The value so obtained may then be compared with the momentum per unit mass in the binary. Suppose the ratio between these momenta is Q. We shall show that, *if* $Q > 5/3$, *the period will decrease;* if $Q < 5/3$, the period of the binary will increase.

Taking as units the mass of the sun, the astronomical unit, and the year, we have

$$\frac{a^3}{P^2} = M \; ; \qquad v = \frac{2\pi a}{P} \; ; \qquad \text{and } \mathcal{M} = \mu(1-\mu)Mav \, , \tag{61}$$

in which M is the total mass and $\mathcal{M}$ the total momentum of the binary. Eliminating a and v, we have

$$\mathcal{M} = 2\pi\mu(1-\mu)M^{5/3}P^{1/3} \, . \tag{62}$$

Keeping the mass ratio constant, we obtain

$$\frac{d\mathcal{M}}{\mathcal{M}} = \frac{5}{3}\frac{dM}{M} + \frac{1}{3}\frac{dP}{P} \, . \tag{63}$$

By definition

$$\frac{-d\mathcal{M}}{-dM} : \frac{\mathcal{M}}{M} = Q \; ; \tag{64}$$

hence, by (63)

$$\frac{dP}{P} = 3(Q - \tfrac{5}{3})\frac{dM}{M} \, . \tag{65}$$

Since dM is negative, dP will be negative if $Q > 5/3$. The fact that we have kept μ constant is no restriction to our discussion, as the effect of a variable mass ratio is examined under (*a*) above.

[50] *Ap. J.*, **89**, 526, 1939.

From equation (58) we find the velocities X and Y valid for a nonrotating frame having the same instantaneous position as the rotating frame; X, Y, x, and y therefore determine the momentum per unit mass. We find 1.76 for the orbit with $v_0 = 0.1$, and 1.78 for the orbit with $v_0 = 0.53$. In the same units the orbital momentum in the binary is, per unit mass, $(1 - \mu)\,\mu^2 + \mu(1 - \mu)^2 = \mu(1 - \mu) = 0.24$ if $\mu = 0.4$. Hence, $Q \cong 7.4 \gg 5/3$. Hence the period should *decrease* as a result of the ejection.

As is well known, the period has been increasing during the interval of over a century covered by the observations. Of the three causes mentioned above only that under (*c*) might be able to produce such an increase. This question is examined in the addendum to this paper.

Other applications may be made to the W Ursae Majoris stars which seem to be contact binaries composed of two dwarf stars. The shallowness of the minima after correction for ellipticity apparently results from the great extent of the common envelope. The magnitude difference and the ratio in surface brightness should again be abnormally large for the difference in mass, so that from the near-equality of the components in several of these systems almost exact equality of masses must be concluded. The equalization of the masses, discussed in section 2, has in these stars reached, or nearly reached, its final stage. A closer spectroscopic study of the more unequal pairs of this class might show traces of currents around the components.

Ejection of type A seems to be fairly common, as more and more pairs become known which are composed of a large giant and a small hot component, the latter being surrounded by gas that might well have originated in the former, as described in section 4. We refer to such stars as WY Geminorum, W Cephei, Z Andromedae, T Coronae Borealis, and several others recently studied by Merrill[51] and by Swings and Struve.[52]

The case of Antares[53] is somewhat different, because, first, the primary does not nearly fill its first "contact surface" and, second, the orbital motion is probably very small (less than 8 km/sec, depending on the projection factor in the observed separation), not larger than the atomic velocities. Under these circumstances there is no longer a closed surface of zero velocity within which the atoms around B are trapped.

In conclusion, I wish to record my indebtedness to Dr. Struve for several discussions on the spectroscopic data concerning β Lyrae. These discussions have helped materially in finding the significant processes operating in this complex system.

YERKES OBSERVATORY
October 3, 1940

ADDENDUM

CHANGES OF PERIOD IN CONTACT BINARIES

In the preceding pages the influence on the orbital period of the pressure at the interface of the components was mentioned but was not examined numerically. A brief survey of the problem is made below.

1. *The numerical value of the pressure.*—In the dynamical problem to be considered later it is convenient to have the radial repulsive force, caused by the pressure at the interface, expressed in terms of the gravitational attraction between the components. We shall compute the repulsive force for the case of equal components, because in that case the large instabilities, present in unequal components, will be absent, so that von Zeipel's theorem on the distribution of pressure should give a good approximation.

[51] E.g., *Spectra of Long-Period Variable Stars*, chaps. vi and vii, 1940.

[52] *Ap. J.*, **91**, 546, 1940; *Pub. A.S.P.*, **52**, 199, 1940.

[53] *Ap. J.*, **92**, 316, 1940.

The procedure followed is this: By using the Roche model the variation of the potential is found in the yz-plane (the interface) and along the b-axis of one of the (equal) components. It is then assumed that the variation of pressure along the b-axis is the same as that along the radius of a single star having the same mass. Using the theoretical pressures for a polytrope of index 3, the pressure at the interface is computed in terms of the central pressure of the star, $P_c = 11.05\ (GM^2/R^4)$,[54] times an area, so that a comparison is possible with the gravitational attraction, GM^2/r^2, when R is fixed in terms of r. Different ratios of R/r are possible, between the extremes of binaries just in contact and those with envelopes of maximum possible height. Taking b as a good measure of R (cf. Table 3), we find from Table 3 that R/r (i.e., b/r) may vary from 0.374 to 0.482. The repulsive force will be zero in the former case and will have its maximum value in the latter case. Since in the process of mass transfer $\bar{R}$ is nearly constant in absolute measure, the variation of the repulsive force thus found will mean a variation with r; this is the relation needed in the dynamical problem.

TABLE 15

b/r	$-\Omega$	y/r	b/r	$-\Omega$	y/r
0.3740.....	2.0000	0.0000	0.4400.....	1.8158	0.2536
.3800.....	1.9804	.0756	.4600.....	1.7720	.2901
.4000.....	1.9192	.1583	0.4823.....	1.7284	0.3261
0.4200.....	1.8647	0.2112			

For small distances from the x-axis (i.e., in the region where the pressures are largest) the potential on the interface (the yz-plane) is given by

$$-\Omega = 2 - 3\tfrac{1}{2}y^2 - 4z^2 + \text{terms of fourth order, etc.} \qquad (66)$$

Near the x-axis the curves of constant potential are therefore ellipses with axes in the ratio

$$2 : \sqrt{3\tfrac{1}{2}} = 1 : 0.9354\,.$$

We shall make the computations for a circular distribution and afterward multiply by 0.935.

The variation of the potential along the y-axis of the interface and the b-axis of one of the components is given in Table 15. The first and the last lines correspond to the extreme cases of first contact and maximum envelope.

The pressure is now found as follows: Consider, e.g., the last line of Table 15. $R/r = 0.4823$ fixes r, needed in computing the gravitational attraction. The maximum value of P/P_c, found at $y = 0$, equals the value at radius $0.3740/0.4823 = 0.775$ of a single star of the same mass. From the *British Association Mathematical Tables, II*, we find that, for $n = 3$ and $x/x_0 = 0.775$, $P/P_c\ (= B) = 0.51 \cdot 10^{-4}$.

Similarly, the ratio P/P_c may be found for other points at the same interface and also for different values of R/r. Table 16 gives the results. The unit of P/P_c is 10^{-6}.

The total pressure (or repulsive force) at the interface is

$$F = 0.935\, P_c R^2 \int_0^\infty 2\pi \frac{y}{R} \cdot \frac{P}{P_c} \cdot d\left(\frac{y}{R}\right) = g \cdot R^2 P_c\,. \qquad (67)$$

[54] S. Chandrasekhar, *Stellar Structure*, p. 230.

The coefficients g are shown in Table 17; they were obtained by quadratures. The total pressure will be equal to the pressure at the center of the interface times a certain area. If this area is taken to be a circle, its radius, a/R, is found in Table 17. It shows that the central region becomes of increasing relative importance for a smaller degree of contact. Finally, F may now be expressed in terms of the gravitational attraction; if we denote the ratio by f (a dimensionless constant), we have $f = 11.05 \times g \times (r/R)^2$. The values of f are found in Table 17; the maximum is only 1/1800.

The results in Table 17 have been derived for the case of equal components; but we shall use them in the general case as well, since they will probably give a fair approxima-

TABLE 16

	R/r									
	0.4823		0.4600		0.4400		0.4200		0.4000	
y/r	y/R	P/P_c	y/R	P/P_c	y/R	P/P_c	y/R	P/P_c	y/R	P/P_c
0.0000.....	0.0000	51.0	0.0000	20.5	0.0000	7.1	0.0000	1.68	0.0000	0.17
.0756.....	.1567	38.6	.1643	14.4	.1718	4.6	.1800	0.90	.1890	.057
.1583.....	.3282	13.1	.3441	3.7	.3598	0.74	.3769	0.05	0.3958	0.000
.2112.....	.4379	3.5	.4591	0.61	.4800	0.04	0.5029	0.00	.....	.....
.2536.....	.5258	0.63	.5513	0.03	0.5764	0.00	.....	.....	.....	.....
.2901.....	.6015	0.04	0.6306	0.00	.....	.....	.....	.....	.....	.....
0.3261.....	0.6761	0.00	.....	.....	.....	.....	.....	.....	.....	.....

TABLE 17

R/r	$g \cdot 10^6$	a/R	$f \cdot 10^6$	r/R
0.4823.....	11.6	0.27	550	2.073
.4600.....	4.03	.25	210	2.174
.4400.....	1.24	.23	71	2.273
.4200.....	0.23	.21	14.3	2.381
.4000.....	0.014	.16	1.0	2.500
0.3740.....	0.000	0.00	0.00	2.674

tion and since no simple method seems available to determine the pressure between two unequal stars not in equilibrium.

2. *Secular changes of period.*—The first question to examine is whether the secular changes already considered (mass transfer from A to B and ejection), which were found to cause a *decrease* in period if the repulsive force at the interface is neglected, could produce an increase if this force is taken into account. Because of the smallness of the ratio f there seems little reason to expect this.

This expectation is confirmed by the following analysis. We are interested in secular changes of a nearly circular orbit, so that we put $\ddot{r} = 0$ in the equations of motion:

$$0 = r\omega^2 - \frac{M}{r^2}(1 - f), \qquad (68) \qquad \text{or} \qquad r^3\omega^2 = M(1 - f), \qquad (68')$$

and

$$\mu(1 - \mu)Mr^2\omega = \mathcal{M}_6. \qquad (69)$$

Here $M = M_1 + M_2 = (1 - \mu)M + \mu M$, and $\mathcal{M}$ is the total angular momentum of the binary. The first equation expresses the obvious fact that in the equilibrium orbit the sum of the centrifugal force and the repulsive force equals the gravitational attraction; equation (68′) gives the modified third law of Kepler. The second equation (eq. [69]), obtained after one integration, expresses the fact that only radial forces are operating; as the masses are variable, Kepler's law of areas has been replaced by the corresponding momentum integral. If ejection takes place, however, transverse forces will be present; they are automatically taken into account, if now, $\mathcal{M}$ is considered variable and $d\mathcal{M}/dM$ is taken from the theory of ejection. It is noted that the rotational momentum of the components has been neglected. Its effect is mentioned later.

We shall now compare the binary at two epochs, t_0 and t, far enough apart for changes of the first order to have taken place. We put

$$\left.\begin{aligned} \frac{r}{r_0} &= 1 + \delta\,, & \frac{M}{M_0} &= 1 + \beta,\\ \frac{\omega}{\omega_0} &= 1 + \epsilon\,, & \frac{\mathcal{M}}{\mathcal{M}_0} &= 1 + Q\beta\,,\\ \frac{\mu}{\mu_0} &= 1 + \lambda\,, & f &= f_0 + \varphi\,, \end{aligned}\right\} \tag{70}$$

in which the increments are proportional to the interval, $(t - t_0) = \Delta t$. (Hence, $\delta = [1/r_0]\,[dr/dt]\Delta t$, etc.) We know β to be negative or zero; its amount is known in principle. The ratio Q was defined on page 171 and was found to be about 7.4. Known in principle are also λ, governing the rate of mass transfer, and

$$\varphi = \frac{df}{dt}\,\Delta t = \frac{\partial f}{\partial r}\,\Delta r + \frac{\partial f}{\partial t}\,\Delta t = \frac{\partial f}{\partial r}\cdot r\cdot\delta + \frac{\partial f}{\partial t}\,\Delta t = h(-\delta + \gamma)\,,$$

because $(\partial f/\partial r)\Delta r$ is found from Table 17, and $(\partial f/\partial t)\Delta t$ is known, in principle, after the changes in the radii and masses have been allowed for. There remain the true unknowns, δ and ϵ; they are obtained by the introduction of equation (70) into equations (68) and (69). By differentiating equations (68′) and (69) logarithmically and multiplying by $\Delta t/dt$, we get

$$3\delta + 2\epsilon = \beta - \varphi\,, \tag{71}$$

$$\nu + \beta + 2\delta + \epsilon = Q\beta\,, \qquad \text{if} \qquad \nu = \lambda\,\frac{1 - 2\mu_0}{1 - \mu_0} \gtrless 0\,. \tag{72}$$

Solving equations (71) and (72) for δ and ϵ, we find

$$\left.\begin{aligned} \delta &= \frac{(2Q - 3)\beta - 2\nu + h\gamma}{1 + h}\,,\\ \epsilon &= \frac{-\{3Q - 5 - (Q - 1)h\}\beta + (3 - h)\nu - 2h\gamma}{1 + h}\,. \end{aligned}\right\} \tag{73}$$

The critical value of $Q = 5/3$ for the change of the period is confirmed by these general formulae; with $Q > 5/3$, ejection ($\beta < 0$) leads to a positive value of ϵ, as does mass transfer ($\nu > 0$). We found $Q \cong 7.4$.

The maximum value of h occurs in the first interval of Table 17; from $\Delta f = -h(\Delta r/r)$ we find for the mean value in this interval, $h = +0.0050$. For the four successive intervals the mean values are $+0.0031$, $+0.0012$, $+0.00027$, and $+0.000015$. The changes in the sum of the radii will in general be small compared to the change in distance between the components. The change of the repulsive force is, therefore, in general due chiefly to the latter cause; or $h\gamma \ll h\delta$ and may be entirely neglected in equation (73). Since $h \lll 3$ and $h \lll (3Q - 5)/(Q - 1) \cong 2.7$, we must conclude that *the period of a contact binary should secularly decrease despite the pressure at the interface.* The only escape from this conclusion provided by equation (73) is a rather sudden increase in the stellar diameter(s), causing a large value of γ during a limited interval. But such an increase in diameter would soon cause an increase in the rotational momentum of the stars (which was neglected in the derivation of eq. [73]), resulting in a decrease of the orbital period. In view of the weakness of the repulsive force, this opposite effect may well preponderate; so that a sudden *decrease* of the diameters might temporarily reverse the general trend of a decreasing period.

If the masses are very nearly equal ($\nu \leqq 0$) and if no ejection takes place ($\beta = 0$), as is probably the case for several W UMa stars, the period should remain secularly constant, unless changes occur in the stellar diameters.

3. *Periodic variations of period.*—Since we shall now consider fluctuations in r over shorter intervals, we have to retain $\ddot{r}$ in the equations of motion but may neglect the mass transfer and the ejection. The equations of motion are now (the second one after one integration):

$$\left.\begin{aligned} \ddot{r} &= r\dot{\theta}^2 - \frac{M}{r^2}(1 - f)\,, \\ r^2\dot{\theta} &= h\,. \end{aligned}\right\} \tag{74}$$

We eliminate $\dot{\theta}$ and obtain

$$\ddot{r} = \frac{h^2}{r^3} - \frac{M}{r^2} + \frac{MN}{r^2}\, e^{-sr/R}\,. \tag{75}$$

Here we have replaced f by an exponential relation found from Table 17: $\log f = 7.15 - 5(r/R)$, which represents the most important interval, $2.07 < r/R < 2.4$, quite well. We have, therefore, $N = 10^{7.15}$ and $s = (5/\mathrm{Mod}) = 11.5$.

The oscillations of r determined by equation (75) are most readily obtained by a perturbation method. If the orbit were circular, its radius would be found from equation (75) by putting $\ddot{r} = 0$ and $r = a$, the latter being the radius of the orbit. We shall refer to equation (75) in this form as equation (75′). Considering small oscillations, we put $r = a(1+\alpha)$; hence $\ddot{r} = a\ddot{\alpha}$, and from equation (75)

$$\ddot{\alpha} = -\alpha B^2\,, \tag{76}$$

$$\text{if} \qquad B^2 = 3\frac{h^2}{a^4} - 2\frac{M}{a^3} + \left(s\frac{a}{R} + 2\right)\frac{MN}{a^3}\, e^{-s\alpha/R}\,. \tag{77}$$

The solution of equation (76) is $\alpha = A \sin(Bt + \varphi)$, in which the semiamplitude, A, and the phase, φ, are arbitrary and the period of the oscillation is $2\pi/B$.

In order to see the relative importance of the terms in equation (77), we put first $N = 0$. From equation (75′) we then find $h^2/a^4 = M/a^3$, so that $B^2 = M/a^3$. Kepler's third law for the orbit gives $\omega^2 = M/a^3$. Hence, $B = \omega$, or the period of the oscillation

equals that of the period in the circular orbit. We obtain, therefore, motion in a stationary ellipse.

In the presence of the repulsive force equation (75′), or (74), gives as Kepler's third law:

$$\omega^2 = \frac{M}{a^3}(1 - f_0) ; \tag{78}$$

whereas from equations (77) and (75′) we find

$$B^2 = \frac{M}{a^3}\left[1 + \left(s\frac{a}{R} - 1\right)f_0\right] . \tag{79}$$

Here f_0 is the value of f at $r = a$, the mean radius of the orbit. Hence, if Π is the period of the oscillation and P that of the circular orbit, we find

$$\frac{\Pi}{P} = \frac{\omega}{B} = 1 - \frac{saf_0}{2R} . \tag{80}$$

For s we found 11.5; for a we may put the mean value $2.2R$; the coefficient of f_0 is therefore about -12.6. Since f_0 is, at most, about 0.00055 (cf. Table 17), we find that *the only effect of the repulsive force is a slow regression of the line of apsides*. The period P' of the rotation of the apse is

$$\frac{P'}{P} = \left(\frac{saf_0}{2R}\right)^{-1} \cong (12.6f_0)^{-1} > 152 . \tag{81}$$

The period P' is independent of the eccentricity of the orbit as long as e remains a quantity of the first order. (The ratio 152 is based on the correct limiting value of a, not on the mean value.) The effect (eq. [81]) will complicate the derivation of the density concentration from the rotation of the line of apsides whenever the components are in contact; and contact will exist if $R/r > 0.374$, in which R is the true (not necessarily the photometrically determined) radius.

Summary.—In the first section the repulsive force caused by the pressure at the interface of a contact binary is evaluated numerically for the case of equal components. The result is found in Table 17, in which f expresses the repulsive force, for different distances r/R, in terms of the gravitational attraction between the components. Next, secular changes of period are examined; it is found that the repulsive force does not materially change the rate of decrease of period caused by ejection of matter or mass transfer from A to B. Periodic changes are found to be limited to a rotation of the line of apsides, the period of which is given by equation (81). The conclusion is that only changes in the stellar radii can temporarily lead to an increase of the orbital period.

October 12, 1940